A Convergent Conformal Energy Minimization for the Computation of Disk Parameterizations*

Yueh-Cheng Kuo†, Wen-Wei Lin‡, Mei-Heng Yueh§, and Shing-Tung Yau¶

Abstract. Surface conformal parameterizations have been widely applied to various tasks in computer graphics. In this paper, we develop a convergent conformal energy minimization (CCEM) iterative algorithm via the line-search gradient descent method with a quadratic approximation for the computation of disk-shaped conformal parameterizations of simply connected open triangular meshes. In addition, we prove the global convergence of the proposed CCEM iterative algorithm. Moreover, under some mild assumptions, we prove the existence of the nontrivial solution, which is a local minimum of the conformal energy with a bijective boundary map. Numerical experiments indicate that the efficiency of the proposed CCEM algorithm is highly improved and the accuracy is competitive with that of state-of-the-art algorithms.

Key words. disk conformal parameterization, conformal energy minimization, simply connected open surface

AMS subject classifications. 15B48, 52C26, 65F05, 68U05, 65D18

1. Introduction.

A conformal parameterization of a surface refers to an angle-preserving diffeomorphism that maps the surface to a planar domain of a canonical shape. The computation of surface conformal parameterizations aims to develop efficient and robust algorithms for computing a conformal diffeomorphism that maps a surface to a canonical planar domain. A global coordinate system on the surface is induced by the inverse map of the parameterization, which can be applied to simplify various tasks in computer graphics, such as surface registration, resampling, remeshing, fusion, and texture mapping.

Classical computational methods for surface conformal parameterizations include the circle packing method [36, 24], the linear Laplace–Beltrami equation [6, 20], the angle-based flattening method [33, 34], the least squares conformal map [27], the holomorphic 1-form method [16, 17, 26], spectral conformal parameterization [29, 23], heat diffusion [15, 22], the discrete Ricci flow [25, 39], the quasi-conformal approach [10], and boundary first flattening [32]. More details about the development of algorithms and applications of surface parameterization can be found in several classical survey papers [13, 35, 21, 5, 14, 19]. Recently, Choi et al. [8] proposed an efficient parallelizable algorithm for the computation of conformal parameterizations. In this paper, we focus on the development of CPU-based algorithms.

In particular, for a simply connected open Riemann surface, the uniformization theorem

*Submitted to the editors DATE.

Funding: The work of the authors was partially supported by the Ministry of Science and Technology, the National Center for Theoretical Sciences, the ST Yau Center in Taiwan, the Nanjing Center for Applied Mathematics, and the Center of Mathematical Sciences and Applications at Harvard University.

†Department of Applied Mathematics, National University of Kaohsiung, Kaohsiung, Taiwan (yckuo@nuk.edu.tw).

‡Department of Applied Mathematics, National Yang Ming Chiao Tung University, Hsinchu, Taiwan, and Nanjing Center for Applied Mathematics, Nanjing 211135, People's Republic of China (wwlin@math.nctu.edu.tw).

§Department of Mathematics, National Taiwan Normal University, Taipei, Taiwan (yue@ntnu.edu.tw).

¶Department of Mathematics, Harvard University, Cambridge, MA 02138, and Nanjing Center for Applied Mathematics, Nanjing 211135, People's Republic of China (yau@math.harvard.edu).

guarantees that the shape of the domain can be a unit disk. The map is known as the Riemann mapping. The computation of the Riemann mapping is a fundamental issue that has been widely studied. Gu and Yau [18, Section 10.4] first proposed a computational algorithm via heat diffusion with the double covering technique. Huang et al. [22] further improved the efficiency of heat diffusion by applying the quasi-implicit Euler method. A year later, Choi and Lui [11] proposed a fast disk conformal parameterization (FDCP) algorithm with improved conformality distortion and computational efficiency based on the composition of two quasi-conformal mappings with the same Beltrami differential. To further improve the efficiency of computations, Choi and Lui [9] developed a linear disk conformal parameterization (LDCP) algorithm based on the double covering technique and the composition of quasi-conformal maps. Noting that the double covering technique would double the size of linear systems and cause computational inefficiency, Yueh et al. [38] developed an efficient algorithm based on the conformal energy minimization (CEM) under the circle boundary constraint with the existence of nontrivial accumulation points guaranteed that does not involve linear systems that are doubled in size. Although the CEM algorithm is effective in computing disk-shaped conformal parameterizations, the convergence of the CEM algorithm has not been completely proved.

In this paper, we aim to develop a convergent CEM (CCEM) algorithm via the line-search gradient descent method with a quadratic approximation for the computation of the conformal map and propose a convergence theory for this new algorithm. The contributions and advantages of the CCEM algorithm are threefold:

- The convergence of the CCEM algorithm is theoretically guaranteed to satisfy the Wolfe and Zoutendijk conditions under some mild assumptions on the Delaunay triangular mesh.
- The existence of a nontrivial local minimizer for the CEM problem having a distinct angle partition on the boundary of the unit disk is proved by keeping the first-order perturbation of Dirichlet energy at zero.
- The computational effectiveness and the conformality accuracy in terms of the conformal energy of the CCEM algorithm are competitive and improved compared to those of other state-of-the-art algorithms.

The notation used in this paper is defined as follows. Bold letters $\mathbf{f}$, $\mathbf{p}$, $\mathbf{q}$ denote (complex-valued) vectors; f_i denotes the ith entry of $\mathbf{f}$; Capital letters A, C, L denote matrices; $L_{i,j}$ denotes the (i,j)th entry of L; Typewriter letters $\mathtt{B}$, $\mathtt{I}$ denote ordered index sets of vertices; $\mathbf{f}_{\mathtt{I}}$, $\mathbf{f}_{\mathtt{B}}$ denote the subvectors of $\mathbf{f}$ composed of $\mathbf{f}_i$ for $i \in \mathtt{I}$ and $i \in \mathtt{B}$, respectively; $L_{\mathtt{I},\mathtt{J}}$ denotes the submatrix of L composed of $L_{i,j}$ for $i \in \mathtt{I}$ and $j \in \mathtt{J}$; $\mathbf{e}_j$ is the jth column of an identity matrix; $\mathrm{diag}(\mathbf{f})$ maps a (complex-valued) vector $\mathbf{f}$ to a diagonal matrix with the (i,i)th entry being f_i; i denotes the imaginary unit $\sqrt{-1}$; $n_{\mathtt{I}}$ is the number of elements of the set $\mathtt{I}$; $\mathbf{0}$ and 0 denote zero vectors and zero matrices, respectively, of appropriate sizes; $\mathbf{1}$ denotes a vector with all entries being 1.

The remainder of this paper is organized as follows. In Section 2, we introduce the background knowledge of conformal maps and conformal energy. In Section 3, we introduce the discretization of Riemann surfaces and mappings by Delaunay triangular meshes and derive the discrete version of the CEM. Then, in Section 4, we develop a line-search gradient descent method with quadratic approximation, called the CCEM algorithm, for the CEM problem

and illustrate its convergence. A proof of the existence of the nontrivial local minimum of the proposed CCEM algorithm is demonstrated in Section 5. We compare the numerical results of the CCEM algorithm and other state-of-the-art algorithms in Section 6. Finally, concluding remarks are given in Section 7.

2. Conformal maps and CEMs. Let $\mathcal{S}_1 = r_1(u_1, v_1)$ and $\mathcal{S}_2 = r_2(u_2, v_2)$ be two 2D Riemann surfaces with I_1 and I_2 being the associated first fundamental forms, respectively. A diffeomorphism $f : \mathcal{S}_1 \to \mathcal{S}_2$ is said to be conformal (i.e., angle-preserving) if it satisfies $f^*\mathrm{I}_2 = \lambda^2 \mathrm{I}_1$, where $f^*\mathrm{I}_2$ is the pullback metric induced by f [37]. Here, the positive scalar factor λ^2 is known as the conformal factor with respect to the conformal map f. The renowned Poincare–Klein–Koebe uniformization theorem asserts that a simply connected 2D Riemann surface is conformally equivalent to one of the following three canonical Riemann surfaces (i) $\overline{\mathbb{C}} = \mathbb{C} \cup \{\infty\}$; (ii) $\mathbb{C}$; (iii) $\mathbb{D} = \{z \in \mathbb{C} \mid |z| \leqslant 1\}$.

Let $\mathcal{M} = r(u, v)$ be a 2D Riemann surface with a single boundary $\partial\mathcal{M}$. From the uniformization theorem, it holds that there is a conformal map $f \equiv (f^1, f^2) : \mathcal{M} \to \mathbb{D}$. If we choose orthogonal coordinate systems for $\mathcal{M}$ and $\mathbb{D}$ such that the first fundamental forms of $\mathcal{M}$ and $\mathbb{D}$ become $\mathrm{I}_1 = \mathrm{d}u^2 + \mathrm{d}v^2$ and $\mathrm{I}_2 = (\mathrm{d}f^1)^2 + (\mathrm{d}f^2)^2$, respectively, then

$$\begin{aligned} f^*\mathrm{I}_2 &= [\mathrm{d}u, \mathrm{d}v] J \begin{bmatrix} 1 & 0 \\ 0 & 1 \end{bmatrix} J^\top \begin{bmatrix} \mathrm{d}u \\ \mathrm{d}v \end{bmatrix} \\ &= |f_u|^2 \mathrm{d}u^2 + 2 f_u \cdot f_v \mathrm{d}u\mathrm{d}v + |f_v|^2 \mathrm{d}v^2, \end{aligned} \tag{2.1}$$

where $J = \begin{bmatrix} \frac{\partial f^1}{\partial u} & \frac{\partial f^2}{\partial u} \\ \frac{\partial f^1}{\partial v} & \frac{\partial f^2}{\partial v} \end{bmatrix} \equiv \begin{bmatrix} f_u^1 & f_u^2 \\ f_v^1 & f_v^2 \end{bmatrix}$. From the computational perspective, we define the Dirichlet energy as

$$E_D(f) = \frac{1}{2} \int_{\mathcal{M}} (|\nabla f^1|^2 + |\nabla f^2|^2) \mathrm{d}u\mathrm{d}v = \frac{1}{2} \int_{\mathcal{M}} (|f_u|^2 + |f_v|^2) \mathrm{d}u\mathrm{d}v \tag{2.2}$$

and let $A(f)$ be the area of the image of f. Then, we have

$$\begin{aligned} \pi = A(f) &= \int_{\mathcal{M}} |f_u \times f_v| \mathrm{d}u\mathrm{d}v \leqslant \int_{\mathcal{M}} |f_u||f_v| \mathrm{d}u\mathrm{d}v \leqslant \frac{1}{2} \int_{\mathcal{M}} (|f_u|^2 + |f_v|^2) \mathrm{d}u\mathrm{d}v \\ &= E_D(f). \end{aligned} \tag{2.3}$$

We define the conformal energy $E_C(f)$ as the difference between $E_D(f)$ and $A(f)$ by

$$E_C(f) = E_D(f) - A(f) \geqslant 0. \tag{2.4}$$

Then, $E_C(f) = 0$, i.e., the equalities in (2.3) hold. This is equivalent to $|f_u| = |f_v|$ and $f_u \cdot f_v = 0$. From (2.1), we obtain that $f^*\mathrm{I}_2 = \lambda^2(\mathrm{d}u^2 + \mathrm{d}v^2) = \lambda^2 \mathrm{I}_1$ with $\lambda^2 = |f_u|^2$. This implies that f is conformal. Hence, finding a conformal map $f : \mathcal{M} \to \mathbb{D}$ is equivalent to solving the optimization problem.

$$\min_{f:\mathcal{M}\to\mathbb{D}} \{E_C(f) \mid f \text{ is bijective}\}. \tag{2.5}$$

Every conformal map is harmonic [13]. Once the boundary condition $f|_{\partial\mathcal{M}} = f_b : \partial\mathcal{M} \to \partial\mathbb{D}$ is given, the map can be uniquely determined by solving the following Laplace–Beltrami equation [31].

$$\begin{cases} \triangle_{\mathcal{M}} f = 0 \text{ on } \mathcal{M}\backslash\partial\mathcal{M}, \\ f|_{\partial\mathcal{M}} = f_b. \end{cases} \tag{2.6}$$

Since there are infinitely many possible choices for boundary map f_b, it is, in general, difficult to find the optimal boundary condition f_b.

3. Discrete version of CEMs. A discretized version of a 2D Riemann surface $\mathcal{M}$ is a Delaunay triangular mesh [18, Chapter 10] composed of an ordered vertex set $\mathcal{V}(\mathcal{M})$, an edge set $\mathcal{E}(\mathcal{M})$ and a triangular face set $\mathcal{F}(\mathcal{M})$ such that (i) the circumcircle of any triangle does not enclose vertices other than the three vertices of the triangle; (ii) the subgraph on all interior vertices/boundary vertices is connected and every boundary vertex is connected to at least one interior vertex. Furthermore, hereafter, the triangular mesh $\mathcal{M}$ we consider is a simply connected open surface with a single boundary that satisfies (i) and (ii).

Let $\mathcal{V}(\mathcal{M}) = \{v_s \in \mathbb{R}^3 \mid s \in \mathtt{I}\cup\mathtt{B}\}$ be $\tilde{n}$ ordered vertices of $\mathcal{M}$, where $\mathtt{I}$ and $\mathtt{B}$ are index sets of interior and boundary vertices, respectively, and $\tilde{n} = n_{\mathtt{I}} + n \equiv \#(\mathtt{I}) + \#(\mathtt{B})$. A piecewise linear map $f : \mathcal{M} \to \mathbb{D}$ can be expressed by a complex-valued vector

$$\mathbf{f} = \mathbf{f}^1 + \mathrm{i}\,\mathbf{f}^2 = [f(v_1), \ldots, f(v_{\tilde{n}})]^\top \equiv [f_1, \ldots, f_{\tilde{n}}]^\top \in \mathbb{C}^{\tilde{n}}, \tag{3.1}$$

where $f_s = f_s^1 + \mathrm{i}\, f_s^2$, $s = 1, \ldots, \tilde{n}$. The discrete Dirichlet energy [11] on $\mathbf{f}$ is given by

$$E_D(\mathbf{f}) = -\frac{1}{2} \sum_{[v_i, v_j] \in \mathcal{E}(\mathcal{M})} w_{ij} |f_i - f_j|^2 = \frac{1}{2}\, \mathbf{f}^{\mathsf{H}} L\, \mathbf{f}, \tag{3.2a}$$

where $L = [w_{ij}]$,

$$w_{ij} = \begin{cases} -\cot\theta_{ij}, & [v_i, v_j] \in \mathcal{E}(\partial\mathcal{M}), \\ -\frac{1}{2}(\cot\theta_{ij} + \cot\theta_{ji}), & [v_i, v_j] \in \mathcal{E}(\mathcal{M}\backslash\partial\mathcal{M}), \\ -\sum_{\ell \in N_i} w_{i\ell}, & i = j, N_i = \{\ell \mid [v_i, v_\ell] \in \mathcal{E}(\mathcal{M})\}, \end{cases} \tag{3.2b}$$

and θ_{ij}, θ_{ji} are two angles opposite to the edge $[v_i, v_j]$. Note that L in (3.2) is referred to as a discrete Laplacian operator. Since $\mathcal{M}$ is a Delaunay triangular mesh, $\theta_{ij} + \theta_{ji} < \pi$ for $[v_i, v_j] \in \mathcal{E}(\mathcal{M})$. Therefore,

$$w_{ij} = -\frac{1}{2}(\cot\theta_{ij} + \cot\theta_{ji}) = -\frac{\sin(\theta_{ij} + \theta_{ji})}{2\sin\theta_{ij}\sin\theta_{ji}} < 0. \tag{3.3}$$

It follows that matrix L in (3.2) is a singular and irreducible M-matrix with $L\mathbf{1} = \mathbf{0}$. Hence, matrix L has rank $\tilde{n} - 1$. Similar to (2.4), the discrete conformal energy is defined by

$$E_C(\mathbf{f}) = E_D(\mathbf{f}) - A(\mathbf{f}), \tag{3.4}$$

where

$$A(\mathbf{f}) = \frac{1}{2} \sum_{[v_i,v_j]\in\mathcal{E}(\partial\mathcal{M})} |f_i^1 f_j^2 - f_j^1 f_i^2|. \tag{3.5}$$

Furthermore, by means of a suitable reordering of the indices of vertices, matrix L in (3.2) and the complex-valued vector $\mathbf{f}$ can be written as

$$L = \begin{bmatrix} L_{\mathtt{I},\mathtt{I}} & L_{\mathtt{I},\mathtt{B}} \\ L_{\mathtt{I},\mathtt{B}}^\top & L_{\mathtt{B},\mathtt{B}} \end{bmatrix} \text{ and } \mathbf{f} = \begin{bmatrix} \mathbf{f}_\mathtt{I} \\ \mathbf{f}_\mathtt{B} \end{bmatrix}, \tag{3.6}$$

respectively, where $\mathbf{f}_\mathtt{I} \in \mathbb{C}^{n_\mathtt{I}}$, $\mathbf{f}_\mathtt{B} \in \mathbb{C}^n$. For a given boundary condition $\mathbf{f}_\mathtt{B} \subseteq \partial\mathbb{D}$, the discrete Laplace–Beltrami equation associated with (2.6) can be expressed as the linear system

$$L_{\mathtt{I},\mathtt{I}}\mathbf{f}_\mathtt{I} = -L_{\mathtt{I},\mathtt{B}}\mathbf{f}_\mathtt{B}, \tag{3.7}$$

where $L_{\mathtt{I},\mathtt{I}}$ is known as a nonsingular irreducible M-matrix. From (3.2b) and (3.7), it follows that

$$w_{ii} = -\sum_{j\in N_i} w_{ij} \Leftrightarrow f_i \equiv f(v_i) = \sum_{j\in N_i} \left(\frac{-w_{ij}}{w_{ii}}\right) f_j, \tag{3.8}$$

for $i \in \mathtt{I}$ and $f_i \in \mathbb{D}\backslash\partial\mathbb{D}$. Thus, $\mathbf{f} : \mathcal{V}(\mathcal{M}) \to \mathcal{V}(\mathbb{D})$ is a piecewise linear and convex combination mapping. From [12], it follows that $\mathbf{f}$ is one-to-one.

From (3.4), (3.5), and (3.8), the discrete version of the optimization problem (2.5) can be formulated as the CEM problem

$$\min\{E_C(\mathbf{f}) \mid \mathbf{f} : \mathcal{V}(\mathcal{M}) \to \mathcal{V}(\mathbb{D}) \text{ is bijective}\}. \tag{3.9}$$

Let $\boldsymbol{\theta} = (\theta_1, \ldots, \theta_n)^\top$ with $0 \leqslant \theta_1 \leqslant \cdots \leqslant \theta_n \leqslant 2\pi$ and let

$$\mathbf{f}_\mathtt{I} = \mathbf{f}_\mathtt{I}^1 + \mathrm{i}\mathbf{f}_\mathtt{I}^2 \in \mathbb{C}^{n_I}, \quad \mathbf{f}_\mathtt{B} = \mathbf{f}_\mathtt{B}^1 + \mathrm{i}\mathbf{f}_\mathtt{B}^2 \in \mathbb{C}^n \tag{3.10a}$$

with

$$\mathbf{f}_\mathtt{B}^1 \equiv \mathbf{p} = \cos\boldsymbol{\theta} \equiv [\cos\theta_1, \ldots, \cos\theta_n]^\top, \quad \mathbf{f}_\mathtt{B}^2 \equiv \mathbf{q} = \sin\boldsymbol{\theta} \equiv [\sin\theta_1, \ldots, \sin\theta_n]^\top. \tag{3.10b}$$

From (3.5), we see that the area of the inscribed polygon formed by the boundary points $\{(\cos\theta_j, \sin\theta_j)\}_{j=1}^n$ is

$$\begin{aligned} A(\mathbf{f}) &= \frac{1}{2}\sum_{j=1}^{n} \sin(\theta_{j+1} - \theta_j) \\ &= \frac{1}{2} \begin{bmatrix} \cos\theta_1 \\ \cos\theta_2 \\ \vdots \\ \cos\theta_n \end{bmatrix}^\top \begin{bmatrix} 0 & 1 & & -1 \\ -1 & \ddots & \ddots & \\ & \ddots & \ddots & 1 \\ 1 & & -1 & 0 \end{bmatrix} \begin{bmatrix} \sin\theta_1 \\ \sin\theta_2 \\ \vdots \\ \sin\theta_n \end{bmatrix} \equiv \frac{1}{2}\mathbf{p}^\top C\mathbf{q}, \end{aligned} \tag{3.11}$$

where $\theta_{n+1} := \theta_1$. According to (3.1), (3.2a), (3.4), (3.6), and (3.10)–(3.11), the conformal energy can be rewritten as

$$\begin{aligned} E_C(\mathbf{f}) \equiv E_C(\mathbf{f}_{\mathtt{I}}^1, \mathbf{f}_{\mathtt{I}}^2, \boldsymbol{\theta}) &= \frac{1}{2}\mathbf{f}^{\mathsf{H}} L \mathbf{f} - \frac{1}{2}\mathbf{p}^\top C \mathbf{q} \\ &= \frac{1}{2}\left(\mathbf{f}_{\mathtt{I}}^{1\top} L_{\mathtt{I},\mathtt{I}} \mathbf{f}_{\mathtt{I}}^1 + \mathbf{f}_{\mathtt{I}}^{2\top} L_{\mathtt{I},\mathtt{I}} \mathbf{f}_{\mathtt{I}}^2 + \mathbf{p}^\top L_{\mathtt{B},\mathtt{B}} \mathbf{p} + \mathbf{q}^\top L_{\mathtt{B},\mathtt{B}} \mathbf{q} - \mathbf{p}^\top C \mathbf{q}\right) \\ &\quad + \mathbf{f}_{\mathtt{I}}^{1\top} L_{\mathtt{I},\mathtt{B}} \mathbf{p} + \mathbf{f}_{\mathtt{I}}^{2\top} L_{\mathtt{I},\mathtt{B}} \mathbf{q}. \end{aligned} \tag{3.12}$$

Then, $\nabla E_C(\mathbf{f}_{\mathtt{I}}^1, \mathbf{f}_{\mathtt{I}}^2, \boldsymbol{\theta}) = \mathbf{0}$ can be calculated as

$$\begin{bmatrix} L_{\mathtt{I},\mathtt{I}} & 0 & L_{\mathtt{I},\mathtt{B}} & 0 \\ 0 & L_{\mathtt{I},\mathtt{I}} & 0 & L_{\mathtt{I},\mathtt{B}} \\ -\operatorname{diag}(\mathbf{q}) L_{\mathtt{I},\mathtt{B}}^\top & \operatorname{diag}(\mathbf{p}) L_{\mathtt{I},\mathtt{B}}^\top & -\operatorname{diag}(\mathbf{q}) L_{\mathtt{B},\mathtt{B}} + \frac{1}{2}\operatorname{diag}(\mathbf{p}) C & \operatorname{diag}(\mathbf{p}) L_{\mathtt{B},\mathtt{B}} + \frac{1}{2}\operatorname{diag}(\mathbf{q}) C \end{bmatrix} \begin{bmatrix} \mathbf{f}_{\mathtt{I}}^1 \\ \mathbf{f}_{\mathtt{I}}^2 \\ \mathbf{p} \\ \mathbf{q} \end{bmatrix} = \mathbf{0}. \tag{3.13}$$

This implies

$$\mathbf{f}_{\mathtt{I}}^1 = -L_{\mathtt{I},\mathtt{I}}^{-1} L_{\mathtt{I},\mathtt{B}} \mathbf{p}, \quad \mathbf{f}_{\mathtt{I}}^2 = -L_{\mathtt{I},\mathtt{I}}^{-1} L_{\mathtt{I},\mathtt{B}} \mathbf{q}, \tag{3.14a}$$

and

$$\begin{aligned} &-\operatorname{diag}(\mathbf{q}) L_{\mathtt{I},\mathtt{B}}^\top \mathbf{f}_{\mathtt{I}}^1 + \operatorname{diag}(\mathbf{p}) L_{\mathtt{I},\mathtt{B}}^\top \mathbf{f}_{\mathtt{I}}^2 - \operatorname{diag}(\mathbf{q}) L_{\mathtt{B},\mathtt{B}} \mathbf{p} + \operatorname{diag}(\mathbf{p}) L_{\mathtt{B},\mathtt{B}} \mathbf{q} \\ &\qquad + \frac{1}{2}\operatorname{diag}(\mathbf{p}) C \mathbf{p} + \frac{1}{2}\operatorname{diag}(\mathbf{q}) C \mathbf{q} = \mathbf{0}. \end{aligned} \tag{3.14b}$$

Let

$$A = L_{\mathtt{B},\mathtt{B}} - L_{\mathtt{I},\mathtt{B}}^\top L_{\mathtt{I},\mathtt{I}}^{-1} L_{\mathtt{I},\mathtt{B}} \in \mathbb{R}^{n \times n}. \tag{3.15}$$

Since L in (3.6) is a singular irreducible M-matrix, it is easy to check that A is also a singular irreducible M-matrix and the null space of A is $\operatorname{span}\{\mathbf{1}\}$. Equation (3.14b) can be written as

$$-\operatorname{diag}(\mathbf{q}) A \mathbf{p} + \operatorname{diag}(\mathbf{p}) A \mathbf{q} + \frac{1}{2}\operatorname{diag}(\mathbf{p}) C \mathbf{p} + \frac{1}{2}\operatorname{diag}(\mathbf{q}) C \mathbf{q} = \mathbf{0}. \tag{3.16}$$

By substituting (3.14a) into (3.12), the conformal energy can be simplified to

$$E_C(\boldsymbol{\theta}) := E_C(\mathbf{f}) = \frac{1}{2}\mathbf{p}^\top A \mathbf{p} + \frac{1}{2}\mathbf{q}^\top A \mathbf{q} - \frac{1}{2}\mathbf{p}^\top C \mathbf{q}, \tag{3.17}$$

where $\mathbf{p} = \cos\boldsymbol{\theta}$ and $\mathbf{q} = \sin\boldsymbol{\theta}$. Then, the CEM problem in (3.9) becomes

$$\min\{E_C(\boldsymbol{\theta}) \mid 0 \leqslant \theta_1 < \cdots < \theta_n < 2\pi\}. \tag{3.18}$$

The complex-valued vector $\mathbf{f}$ in (3.9) is a vector representation of the piecewise linear map $f : \mathcal{M} \to \mathbb{D}$. From the first-order approximation of the conformal energy in (2.4), it follows that $\mathbf{f}^*$ is a conformal map if and only if there exists $\boldsymbol{\theta}^* = (\theta_1^*, \ldots, \theta_n^*)^\top$ with $0 \leqslant \theta_1^* < \theta_2^* <$

$\cdots < \theta_n^* < 2\pi$ such that $\boldsymbol{\theta}^* = \operatorname{argmin} E_C(\boldsymbol{\theta}) \geqslant 0$ as in (3.18) (or $\mathbf{f}^* = \operatorname{argmin} E_C(\mathbf{f})$ as in (3.9)).

Suppose $E_C(\boldsymbol{\theta})$ in (3.17) has a local minimum $\boldsymbol{\theta}^*$ with $0 \leqslant \theta_1^* < \theta_2^* < \cdots < \theta_n^* < 2\pi$ and let $0 < \varepsilon < \min_{1\leqslant j\leqslant n} |\theta_{j+1}^* - \theta_j^*|$. Then, from the Karush–Kuhn–Tucker (KKT) condition, it holds that

$$\nabla_{\boldsymbol{\theta}} E_C(\boldsymbol{\theta}^*) + \sum_{j=1}^{n} \mu_j^* \nabla_{\boldsymbol{\theta}} (\theta_{j+1}^* - (\theta_j^* + \varepsilon)) = \mathbf{0} \tag{3.19a}$$

and

$$\mu_j^* (\theta_{j+1}^* - (\theta_j^* + \varepsilon)) = 0, \quad j = 1, \ldots, n. \tag{3.19b}$$

From the complementary condition (3.19b), it follows that $\mu_j^* = 0$ for $j = 1, \ldots, n$. Equation (3.19a) then becomes

$$\nabla_{\boldsymbol{\theta}} E_C(\boldsymbol{\theta}^*) = -\operatorname{diag}(\mathbf{q}^*) A \mathbf{p}^* + \operatorname{diag}(\mathbf{p}^*) A \mathbf{q}^* + \frac{1}{2}\operatorname{diag}(\mathbf{p}^*) C \mathbf{p}^* + \frac{1}{2}\operatorname{diag}(\mathbf{q}^*) C \mathbf{q}^* = \mathbf{0}, \tag{3.20}$$

where $\mathbf{p}^* = [\cos\theta_1^*, \ldots, \cos\theta_n^*]^\top$ and $\mathbf{q}^* = [\sin\theta_1^*, \ldots, \sin\theta_n^*]^\top$.

Thus, to find a local minimum $\boldsymbol{\theta}^*$ for $E_C(\boldsymbol{\theta})$ in (3.18), we can solve the optimization problem $\min E_C(\boldsymbol{\theta})$ without considering the constraint of the increasing order of the partition angles.

4. Line-search gradient method and its convergence. We now develop a line-search gradient descent method with a quadratic approximation for solving (3.18). For a given $\mathbf{p} + \mathrm{i}\mathbf{q} = \cos\boldsymbol{\theta} + \mathrm{i}\sin\boldsymbol{\theta} \equiv e^{\mathrm{i}\boldsymbol{\theta}}$, as in (3.20), we compute the negative gradient of $E_C(\boldsymbol{\theta})$ at $\boldsymbol{\theta}$ by

$$\mathbf{d}_{\boldsymbol{\theta}} = -\nabla_{\boldsymbol{\theta}} E_C(\boldsymbol{\theta}) = \operatorname{diag}(\mathbf{q}) A \mathbf{p} - \operatorname{diag}(\mathbf{p}) A \mathbf{q} - \frac{1}{2}\operatorname{diag}(\mathbf{p}) C \mathbf{p} - \frac{1}{2}\operatorname{diag}(\mathbf{q}) C \mathbf{q}. \tag{4.1}$$

Let α be a suitable step-length to be determined. The next iterative angles are given by

$$\boldsymbol{\theta}_\alpha = \boldsymbol{\theta} + \alpha \mathbf{d}_{\boldsymbol{\theta}}. \tag{4.2}$$

The corresponding correction vectors then become

$$\begin{aligned} \mathbf{p}_\alpha + \mathrm{i}\mathbf{q}_\alpha &= e^{\mathrm{i}\boldsymbol{\theta}} \cdot e^{\mathrm{i}\alpha\mathbf{d}_{\boldsymbol{\theta}}} = (\mathbf{p} + \mathrm{i}\mathbf{q}) \cdot (\cos(\alpha\mathbf{d}_{\boldsymbol{\theta}}) + \mathrm{i}\sin(\alpha\mathbf{d}_{\boldsymbol{\theta}})) \\ &= (\mathbf{p} \cdot \cos(\alpha\mathbf{d}_{\boldsymbol{\theta}}) - \mathbf{q} \cdot \sin(\alpha\mathbf{d}_{\boldsymbol{\theta}})) + \mathrm{i}(\mathbf{q} \cdot \cos(\alpha\mathbf{d}_{\boldsymbol{\theta}}) + \mathbf{p} \cdot \sin(\alpha\mathbf{d}_{\boldsymbol{\theta}})), \end{aligned} \tag{4.3}$$

where $\mathbf{u} \cdot \mathbf{v} = [u_1 v_1, \ldots, u_n v_n]^\top$. Consider the Taylor expansions in the vector forms

$$\cos(\alpha\mathbf{d}_{\boldsymbol{\theta}}) = 1 - \frac{1}{2}\alpha^2 \mathbf{d}_{\boldsymbol{\theta}}^2 + O(\alpha^4), \tag{4.4a}$$

$$\sin(\alpha\mathbf{d}_{\boldsymbol{\theta}}) = \alpha\mathbf{d}_{\boldsymbol{\theta}} + O(\alpha^3), \tag{4.4b}$$

where $\mathbf{d}_{\boldsymbol{\theta}}^2 = \mathbf{d}_{\boldsymbol{\theta}} \cdot \mathbf{d}_{\boldsymbol{\theta}}$. According to (4.3) and (4.4), the energy $E_C(\boldsymbol{\theta}_\alpha)$ in (3.17) becomes

$$\begin{aligned} E_C(\boldsymbol{\theta}_\alpha) &= \frac{1}{2}\mathbf{p}_\alpha^\top A\mathbf{p}_\alpha + \frac{1}{2}\mathbf{q}_\alpha^\top A\mathbf{q}_\alpha - \frac{1}{2}\mathbf{p}_\alpha^\top C\mathbf{q}_\alpha \\ &= E_C(\boldsymbol{\theta}) + \alpha\left[-\mathbf{p}^\top A(\mathbf{q}\cdot\mathbf{d}_{\boldsymbol{\theta}}) + \mathbf{q}^\top A(\mathbf{p}\cdot\mathbf{d}_{\boldsymbol{\theta}}) - \frac{1}{2}\mathbf{p}^\top C(\mathbf{p}\cdot\mathbf{d}_{\boldsymbol{\theta}}) + \frac{1}{2}(\mathbf{q}\cdot\mathbf{d}_{\boldsymbol{\theta}})^\top C\mathbf{q}\right] \\ &\quad + \frac{\alpha^2}{2}\left[(\mathbf{q}\cdot\mathbf{d}_{\boldsymbol{\theta}})^\top A(\mathbf{q}\cdot\mathbf{d}_{\boldsymbol{\theta}}) - \mathbf{p}^\top A(\mathbf{p}\cdot\mathbf{d}_{\boldsymbol{\theta}}^2) + (\mathbf{p}\cdot\mathbf{d}_{\boldsymbol{\theta}})^\top A(\mathbf{p}\cdot\mathbf{d}_{\boldsymbol{\theta}}) - \mathbf{q}^\top A(\mathbf{q}\cdot\mathbf{d}_{\boldsymbol{\theta}}^2)\right. \\ &\quad \left. + (\mathbf{q}\cdot\mathbf{d}_{\boldsymbol{\theta}})^\top C(\mathbf{p}\cdot\mathbf{d}_{\boldsymbol{\theta}}) + \frac{1}{2}\mathbf{p}^\top C(\mathbf{q}\cdot\mathbf{d}_{\boldsymbol{\theta}}^2) + \frac{1}{2}(\mathbf{p}\cdot\mathbf{d}_{\boldsymbol{\theta}}^2)^\top C\mathbf{q}\right] + O(\alpha^3) \\ &\equiv E_C(\boldsymbol{\theta}) + \alpha c_1 + \alpha^2 c_2 + O(\alpha^3). \end{aligned} \tag{4.5}$$

The optimal step-length for (4.2) is selected as

$$\alpha = -\frac{c_1}{2c_2} \tag{4.6}$$

which solves the minimal value of the quadratic function $q(\alpha) = E_C(\boldsymbol{\theta}) + \alpha c_1 + \alpha^2 c_2$ in (4.5).

We summarize (4.1)–(4.6) as the following Algorithm 4.1.

Theorem 4.1 (Convergence Theorem). *The line-search gradient method with quadratic approximation in Algorithm 4.1 converges globally.*

Proof. Step 6 in Algorithm 4.1 implies that for $0 \leqslant \alpha \leqslant \alpha'$, it holds that

$$E_C(\boldsymbol{\theta}_k + \alpha\mathbf{d}_{\boldsymbol{\theta}_k}) \leqslant E_C(\boldsymbol{\theta}_k) + \alpha\gamma_1\nabla E_C(\boldsymbol{\theta}_k)^\top\mathbf{d}_{\boldsymbol{\theta}_k}. \tag{4.7}$$

Specifically, inequality (4.7) also holds for $\alpha = 0$. According to the mean value theorem, there is an $\alpha'' \in (0, \alpha')$ such that

$$E_C(\boldsymbol{\theta}_k + \alpha'\mathbf{d}_{\boldsymbol{\theta}_k}) - E_C(\boldsymbol{\theta}_k) = \alpha'\nabla E_C(\boldsymbol{\theta}_k + \alpha''\mathbf{d}_{\boldsymbol{\theta}_k})^\top\mathbf{d}_{\boldsymbol{\theta}_k}.$$

This implies from $0 < \gamma_1 < \gamma_2 < 1$ and $\nabla E_C(\boldsymbol{\theta}_k)^\top\mathbf{d}_{\boldsymbol{\theta}_k} < 0$ that

$$\nabla E_C(\boldsymbol{\theta}_k + \alpha''\mathbf{d}_{\boldsymbol{\theta}_k})^\top\mathbf{d}_{\boldsymbol{\theta}_k} = \gamma_1\nabla E_C(\boldsymbol{\theta}_k)^\top\mathbf{d}_{\boldsymbol{\theta}_k} > \gamma_2\nabla E_C(\boldsymbol{\theta}_k)^\top\mathbf{d}_{\boldsymbol{\theta}_k} \tag{4.8}$$

and there is an open interval $I \subseteq (0, \alpha')$ containing α'' for which α_k determined by Steps 10–20 must exist and lie in I satisfying

$$\nabla E_C(\boldsymbol{\theta}_k + \alpha_k\mathbf{d}_{\boldsymbol{\theta}_k})^\top\mathbf{d}_{\boldsymbol{\theta}_k} > \gamma_2\nabla E_C(\boldsymbol{\theta}_k)^\top\mathbf{d}_{\boldsymbol{\theta}_k}. \tag{4.9}$$

Therefore, the step-length α_k computed in Algorithm 4.1 satisfies the Wolfe conditions (4.7) and (4.9). From (3.17) and (4.1), it is easily seen that $E_C(\boldsymbol{\theta})$ is bounded below and that $\nabla E_C(\boldsymbol{\theta})$ is Lipschitz continuous. Hence, the Zoutendijk condition [30, Section 3.2]

$$\sum_{k\geqslant 0}\cos^2\phi_k\|\nabla E_C(\boldsymbol{\theta}_k)\|^2 < \infty$$

holds, where $\cos\phi_k = \frac{-\nabla E_C(\boldsymbol{\theta}_k)^\top\mathbf{d}_{\boldsymbol{\theta}_k}}{\|\nabla E_C(\boldsymbol{\theta}_k)\|\|\mathbf{d}_{\boldsymbol{\theta}_k}\|}$. Since $\mathbf{d}_{\boldsymbol{\theta}_k} = -\nabla E_C(\boldsymbol{\theta}_k)$, it holds that $\cos\phi_k = 1$. Therefore, we prove the global convergence of the sequence of vectors $\{\nabla E_C(\boldsymbol{\theta}_k)\}_{k=1}^\infty$ as $\lim_{k\to\infty}\|\nabla E_C(\boldsymbol{\theta}_k)\| = 0$. ∎

Algorithm 4.1 Line-search gradient descent method with quadratic approximation

Input: An initial vector $\boldsymbol{\theta}_0 = (\theta_1^0, \ldots, \theta_n^0)^\top$ with $0 = \theta_1^0 < \cdots < \theta_n^0 < 2\pi$, $0 < \gamma_1 < \gamma_2 < 1$, $\rho = 0.99$, and a tolerance $\tau > 0$.

Output: A vector $\boldsymbol{\theta}$.

1: **for** $k = 0, 1, 2, \ldots$ **do**
2: $\quad \mathbf{p}_k = \cos \boldsymbol{\theta}_k$;
3: $\quad \mathbf{q}_k = \sin \boldsymbol{\theta}_k$;
4: $\quad \mathbf{d}_{\boldsymbol{\theta}_k} = \mathbf{d}_{\boldsymbol{\theta}}$ as in (4.1);
5: $\quad \alpha_k = -\frac{c_1}{2c_2}$ as in (4.6);
6: $\quad$ Let α' be the smallest intersecting value of α_k with

$$E_C(\boldsymbol{\theta}_k + \alpha' \mathbf{d}_{\boldsymbol{\theta}_k}) = E_C(\boldsymbol{\theta}_k) + \alpha' \gamma_1 \nabla E_C(\boldsymbol{\theta}_k)^\top \mathbf{d}_{\boldsymbol{\theta}_k};$$

7: $\quad$ **if** $\alpha_k > \alpha'$ **then**
8: $\quad\quad \alpha_k = \alpha'$;
9: $\quad$ **end if**
10: $\quad$ **while** $\nabla E_C(\boldsymbol{\theta}_k + \alpha_k \mathbf{d}_{\boldsymbol{\theta}_k}) \leqslant \gamma_2 \nabla E_C(\boldsymbol{\theta}_k)^\top \mathbf{d}_{\boldsymbol{\theta}_k}$ **do**
11: $\quad\quad \alpha_k \leftarrow \rho \alpha_k$;
12: $\quad\quad$ **if** $\alpha_k \approx 0$ **then**
13: $\quad\quad\quad$ **while** $\nabla E_C(\boldsymbol{\theta}_k + \alpha_k \mathbf{d}_{\boldsymbol{\theta}_k})^\top \mathbf{d}_{\boldsymbol{\theta}_k} \leqslant \gamma_2 \nabla E_C(\boldsymbol{\theta}_k)^\top \mathbf{d}_{\boldsymbol{\theta}_k}$ **do**
14: $\quad\quad\quad\quad \alpha_k \leftarrow \frac{\alpha_k}{\rho}$;
15: $\quad\quad\quad\quad$ **if** $\alpha_k > \alpha'$ **then**
16: $\quad\quad\quad\quad\quad \alpha_k = \alpha'$;
17: $\quad\quad\quad\quad$ **end if**
18: $\quad\quad\quad$ **end while**
19: $\quad\quad$ **end if**
20: $\quad$ **end while**
21: $\quad \boldsymbol{\theta}_{k+1} = \boldsymbol{\theta}_k + \alpha_k \mathbf{d}_{\boldsymbol{\theta}_k}$;
22: $\quad$ **if** $E_C(\boldsymbol{\theta}_k) - E_C(\boldsymbol{\theta}_{k+1}) < \tau$ **then**
23: $\quad\quad$ **break**;
24: $\quad$ **end if**
25: **end for**
26: **return** $\boldsymbol{\theta} = \boldsymbol{\theta}_{k+1}$.

Remark 4.2. To accelerate Algorithm 4.1, the searching gradient direction $d_{\boldsymbol{\theta}_k}$ in Step 4 can be replaced by the quasi-Newton method [7, Chapter 18] as Algorithm 4.2, which is locally convergent, with a convergence rate of 1.618.

5. Existence of the nontrivial local minimum of CEM. In this section, we aim to show the existence of the nontrivial local minimum of CEM having distinct partition angles. Now, we define the energy function with a parameter $\beta \geqslant 0$

$$E_C(\boldsymbol{\theta}; \beta) = \frac{1}{2} \mathbf{p}^\top A \mathbf{p} + \frac{1}{2} \mathbf{q}^\top A \mathbf{q} - \frac{\beta}{2} \mathbf{p}^\top C \mathbf{q}, \tag{5.1}$$

Algorithm 4.2 Quasi-Newton method

Input: Initial vectors $\boldsymbol{\theta}_k = (\theta_1^k, \dots, \theta_n^k)^\top$ with $0 = \theta_1^k < \cdots < \theta_n^k < 2\pi$, $k = 0, 1$.
Output: A vector $\boldsymbol{\theta}$.

$\mathbf{s}_1 = \boldsymbol{\theta}_1 - \boldsymbol{\theta}_0$;
$\mathbf{y}_1 = \nabla E_C(\boldsymbol{\theta}_1) - \nabla E_C(\boldsymbol{\theta}_0)$;
$\delta_1 = \frac{\mathbf{y}_1^\top \mathbf{s}_1}{\mathbf{s}_1^\top \mathbf{s}_1}$;
$H_1 = \delta_1 I$;
for $k = 2, 3, \dots$ **do**
  $\mathbf{s}_k = \boldsymbol{\theta}_k - \boldsymbol{\theta}_{k-1}$;
  $\mathbf{y}_k = \nabla E_C(\boldsymbol{\theta}_k) - \nabla E_C(\boldsymbol{\theta}_{k-1})$;
  $\rho_k = \frac{1}{\mathbf{y}_k^\top \mathbf{s}_k}$;
  $H_k = (I - \rho_k \mathbf{s}_k \mathbf{y}_k^\top) H_{k-1} (I - \rho_k \mathbf{y}_k \mathbf{s}_k^\top) + \rho_k \mathbf{s}_k \mathbf{s}_k^\top$;
  $\mathbf{d}_{\boldsymbol{\theta}_k} = -H_k \nabla E_C(\boldsymbol{\theta}_k)$; ▷ the quasi-Newton direction
  $\boldsymbol{\theta}_{k+1} = \boldsymbol{\theta}_k + \mathbf{d}_{\boldsymbol{\theta}_k}$;
  if $E_C(\boldsymbol{\theta}_k) - E_C(\boldsymbol{\theta}_{k+1}) < \tau$ **then**
    break;
  end if
end for
return $\boldsymbol{\theta} = \boldsymbol{\theta}_{k+1}$.

where $\mathbf{p} = \cos(\boldsymbol{\theta})$ and $\mathbf{q} = \sin(\boldsymbol{\theta})$. Note that $E_C(\boldsymbol{\theta}; 1)$ is the conformal energy $E_C(\boldsymbol{\theta})$ in (3.17). For each $\beta \geqslant 0$, it is easy to check that $E_C(\boldsymbol{\theta}; \beta)$ is invariant under the rotation of $\boldsymbol{\theta}$ by a constant, i.e., $E_C(\boldsymbol{\theta}; \beta) = E_C(\boldsymbol{\theta} + c\mathbf{1}; \beta)$, where $c \in \mathbb{R}$. Then, we consider the optimization problem

$$h(\beta) := \min\{E_C(\boldsymbol{\theta}; \beta) \mid 0 = \theta_1 \leqslant \theta_2 \leqslant \cdots \leqslant \theta_n \leqslant 2\pi\}. \tag{5.2}$$

Note that the feasible region of (5.2) is compact; hence, the minimal value of $E_C(\boldsymbol{\theta}; \beta)$ exists for each $\beta \geqslant 0$. The following lemma shows that $E_C(\boldsymbol{\theta}; \beta)$ has a global minimum at $\mathbf{0}$ when β is sufficiently small.

Lemma 5.1. *The trivial state $\boldsymbol{\theta} = \mathbf{0}$ is a strict local minimizer of (5.2) for all $\beta \geqslant 0$. In addition, there is a $\beta_0 > 0$ such that $h(\beta) = 0$ for $\beta \in [0, \beta_0]$.*

Proof. We choose $\boldsymbol{\theta} = \mathbf{0}$ and then $\mathbf{p} = \mathbf{1}$ and $\mathbf{q} = \mathbf{0}$. Since $A\mathbf{1} = \mathbf{0}$, we have $E_C(\mathbf{0}; \beta) = 0$ for $\beta \geqslant 0$. We consider a small perturbation of $\mathbf{0}$ as $\mathbf{0}_\eta = (\theta_1, \dots, \theta_n)^\top$ with

$$0 = \theta_1 \leqslant \theta_2 = \eta_2 \leqslant \cdots \leqslant \theta_\ell = \eta_\ell < \theta_{\ell+1} = 2\pi - \eta_{\ell+1} \leqslant \theta_n = 2\pi - \eta_n \leqslant 2\pi$$

where $\eta_j \geqslant 0$ are sufficiently small. Let $\eta = \max\{\eta_\ell, \eta_{\ell+1}\} > 0$. Then, $\eta_j \leqslant \eta$ and

$$\begin{aligned} \mathbf{p}_\eta &= \cos(\mathbf{0}_\eta) = [1, 1 - \tfrac{1}{2}\eta_2^2, \dots, 1 - \tfrac{1}{2}\eta_n^2]^\top + O(\eta^4), \\ \mathbf{q}_\eta &= \sin(\mathbf{0}_\eta) = [0, \eta_2, \dots, \eta_\ell, -\eta_{\ell+1}, \dots, -\eta_n]^\top + O(\eta^3). \end{aligned} \tag{5.3}$$

Substituting (5.3) into (5.1), for each $\beta \geqslant 0$, since $\mathbf{q}_\eta \notin \operatorname{span}\{\mathbf{1}\}$, we have

$$\begin{aligned} E_C(\mathbf{0}_\eta;\beta) &= \frac{1}{2}\mathbf{p}_\eta^\top A\mathbf{p}_\eta + \frac{1}{2}\mathbf{q}_\eta^\top A\mathbf{q}_\eta - \frac{\beta}{2}\mathbf{p}_\eta^\top C\mathbf{q}_\eta \\ &= \frac{1}{2}\mathbf{q}_\eta^\top A\mathbf{q}_\eta + O(\eta^3) > 0. \end{aligned} \tag{5.4}$$

This result shows that $\boldsymbol{\theta} = \mathbf{0}$ is a strict local minimizer of (5.2) for all $\beta \geqslant 0$.

For $\beta = 0$, the energy function becomes $E_C(\boldsymbol{\theta};0) = \frac{1}{2}\mathbf{p}^\top A\mathbf{p} + \frac{1}{2}\mathbf{q}^\top A\mathbf{q}$. Since matrix A in (3.15) is semipositive and the null space of A is $\operatorname{span}\{\mathbf{1}\}$, we obtain that $\boldsymbol{\theta} = \mathbf{0}$ is the unique global minimizer of (5.2) with $\beta = 0$. Using the fact that $\boldsymbol{\theta} = \mathbf{0}$ is a strict local minimizer of (5.2) with $\beta \geqslant 0$, there exists $\beta_0 > 0$ such that $h(\beta) = 0$ for $\beta \in [0, \beta_0]$. ∎

Now, we want to show under some mild conditions that the energy function $E_C(\boldsymbol{\theta};\beta)$ has a nontrivial local minimum $\boldsymbol{\theta}^* = (\theta_1^*, \ldots, \theta_n^*)^\top$ with $0 = \theta_1^* < \theta_2^* < \cdots < \theta_n^* < 2\pi$. Let

$$\Theta = \{(\theta_1, \ldots, \theta_n)^\top \mid 0 = \theta_1 \leqslant \theta_2 \leqslant \cdots \leqslant \theta_n \leqslant 2\pi \text{ and } \theta_i < \theta_{i+1} \text{ for some } i\} \tag{5.5}$$

be the set of all angle partitions in nondecreasing order with at least one neighboring pair being distinct. Let $\hat{\boldsymbol{\theta}} = (\hat{\theta}_1, \ldots, \hat{\theta}_n)^\top \in \Theta$, for $s = 1, \ldots, n$; we define

$$\begin{gathered} \boldsymbol{\theta}(s) \equiv (\theta_1, \ldots, \theta_n)^\top \in \Theta \text{ with} \\ \theta_1 = \hat{\theta}_s - \hat{\theta}_s, \ldots,\ \theta_{r-1} = \hat{\theta}_n - \hat{\theta}_s,\ \theta_r = 2\pi + \hat{\theta}_1 - \hat{\theta}_s, \ldots,\ \theta_n = 2\pi + \hat{\theta}_{s-1} - \hat{\theta}_s, \end{gathered} \tag{5.6}$$

where $r \equiv n-s+2 \pmod n$. Note that $\theta_k \equiv \hat{\theta}_{s-1+k} - \hat{\theta}_s \pmod{2\pi}$. For $\boldsymbol{\theta}_0 = (\theta_1, \ldots, \theta_n)^\top \in \Theta$ and $\ell \in \{1, \ldots, n\}$, we denote the perturbation of the angle at θ_ℓ as

$$\boldsymbol{\theta}_{\pm\eta}(\ell) = \begin{cases} (\theta_1, \ldots, \theta_{\ell-1}, \theta_\ell \pm \eta, \theta_{\ell+1}, \ldots, \theta_n)^\top \in \Theta, & \text{if } \ell \neq 1 \\ (\theta_1, \theta_2 \mp \eta, \ldots, \theta_n \mp \eta) \in \Theta & \text{if } \ell = 1, \end{cases} \tag{5.7}$$

where $\eta > 0$. Notably, $\boldsymbol{\theta}_{\pm\eta}(\ell) \in \Theta$ and $E_C(\boldsymbol{\theta}_{\pm\eta}(1), \beta) = E_C(\boldsymbol{\theta}_0 \pm \eta\mathbf{e}_1, \beta)$ for all $\beta \geqslant 0$. We need the following lemma to prove our main results.

Lemma 5.2. *Let $\boldsymbol{\theta}_0 = (\theta_1, \ldots, \theta_n)^\top \in \Theta$. Let $0 < \eta \ll 1$ and $\boldsymbol{\theta}_{\pm\eta}(\ell) \in \Theta$ in (5.7) be an angle partition in nondecreasing order. Then,*

$$\mathbf{p}_{\pm\eta}^\top A\mathbf{p}_{\pm\eta} + \mathbf{q}_{\pm\eta}^\top A\mathbf{q}_{\pm\eta} = \mathbf{p}_0^\top A\mathbf{p}_0 + \mathbf{q}_0^\top A\mathbf{q}_0 \pm 2\eta(\sin(\boldsymbol{\theta}_0 - \theta_\ell\mathbf{1}))^\top \mathbf{a}_\ell + O(\eta^2), \tag{5.8a}$$

$$\mathbf{p}_{\pm\eta}^\top C\mathbf{q}_{\pm\eta} = \mathbf{p}_0^\top C\mathbf{q}_0 + \eta[\mp\cos(\theta_{\ell+1} - \theta_\ell) \pm \cos(\theta_\ell - \theta_{\ell-1})] + O(\eta^2), \tag{5.8b}$$

where $\mathbf{p}_{\pm\eta} = \cos(\boldsymbol{\theta}_{\pm\eta}(\ell))$, $\mathbf{q}_{\pm\eta} = \sin(\boldsymbol{\theta}_{\pm\eta}(\ell))$ and $\mathbf{a}_\ell$ is the ℓ-th column of A.

Proof. $\mathbf{p}_{\pm\eta}$ and $\mathbf{q}_{\pm\eta}$ can be expanded by Taylor expansion as

$$\begin{aligned} \mathbf{p}_{\pm\eta} &= [\cos\theta_1, \ldots, \cos\theta_{\ell-1}, \cos(\theta_\ell \pm \eta), \cos\theta_{\ell+1}, \ldots, \cos(\theta_n)]^\top \\ &= \cos\boldsymbol{\theta}_0 \mp \eta[0, \ldots, 0, \sin\theta_\ell, 0, \ldots, 0]^\top + O(\eta^2), \end{aligned} \tag{5.9a}$$

$$\begin{aligned} \mathbf{q}_{\pm\eta} &= [\sin\theta_1, \ldots, \sin\theta_{\ell-1}, \sin(\theta_\ell \pm \eta), \sin\theta_{\ell+1}, \ldots, \sin(\theta_n)]^\top \\ &= \sin\boldsymbol{\theta}_0 \pm \eta[0, \ldots, 0, \cos\theta_\ell, \ldots, 0]^\top + O(\eta^2), \end{aligned} \tag{5.9b}$$

where $\eta > 0$. Let $\mathbf{p}_0 = \cos\boldsymbol{\theta}_0$ and $\mathbf{q}_0 = \sin\boldsymbol{\theta}_0$; we then obtain

$$\begin{aligned}\mathbf{p}_{\pm\eta}^\top A\mathbf{p}_{\pm\eta} + \mathbf{q}_{\pm\eta}^\top A\mathbf{q}_{\pm\eta} &= \mathbf{p}_0^\top A\mathbf{p}_0 + \mathbf{q}_0^\top A\mathbf{q}_0 + 2\eta(\pm\mathbf{q}_0^\top \mathbf{a}_\ell \cos\theta_\ell \mp \mathbf{p}_0^\top \mathbf{a}_\ell \sin\theta_\ell) + O(\eta^2)\\ &= \mathbf{p}_0^\top A\mathbf{p}_0 + \mathbf{q}_0^\top A\mathbf{q}_0 \pm 2\eta[\sin(\theta_1-\theta_\ell),\dots,\sin(\theta_n-\theta_\ell)]\mathbf{a}_\ell + O(\eta^2)\end{aligned}$$

and

$$\begin{aligned}\mathbf{p}_{\pm\eta}^\top C\mathbf{q}_{\pm\eta} &= \mathbf{p}_0^\top C\mathbf{q}_0 + \eta[\pm\cos\theta_\ell \mathbf{p}_0^\top C\mathbf{e}_\ell \mp \sin\theta_\ell \mathbf{e}_\ell^\top C\mathbf{q}_0] + O(\eta^2)\\ &= \mathbf{p}_0^\top C\mathbf{q}_0 + \eta[\mp\cos(\theta_{\ell+1}-\theta_\ell) \pm \cos(\theta_\ell - \theta_{\ell-1})] + O(\eta^2),\end{aligned}$$

where $\mathbf{a}_\ell$ is the ℓ-th column of A. Hence, (5.8) holds. ∎

Let $\hat{\boldsymbol{\theta}} = (\hat\theta_1,\dots,\hat\theta_n)^\top \in \Theta$, where Θ is defined in (5.5). For each $s \in \{1,\dots,n\}$, we set $\boldsymbol{\theta}_0 \equiv \boldsymbol{\theta}(s) = (\theta_1,\dots,\theta_n)^\top \in \Theta$ as in (5.6) and $r \equiv n-s+2 \pmod n$. For $k \in \{1,\dots,n\}\backslash\{r, r+1\}_{\mathrm{mod}_n}$, we set $\theta_0 = \theta_n - 2\pi$, $\theta_{n+1} = 2\pi$ and define

$$I_+^s = \left\{k \mid \theta_k < \frac{\theta_{k-1}+\theta_{k+1}}{2}\right\},\ I_-^s = \left\{k \mid \theta_k > \frac{\theta_{k-1}+\theta_{k+1}}{2}\right\}, \tag{5.10}$$

and

$$\omega_k(\boldsymbol{\theta}_0) = (\sin(\boldsymbol{\theta}_0 - \theta_k\mathbf{1}))^\top \mathbf{a}_k. \tag{5.11}$$

Here, $\{\cdot\}_{\mathrm{mod}_n}$ denotes the set of $a \pmod n$ for each $a \in \{\cdot\}$. It is easily seen that for each $k \in I_+^s$ (or $k \in I_-^s$), the area of the perturbed polygon of $\mathbf{p}_\eta^\top C\mathbf{q}_\eta$ (or $\mathbf{p}_{-\eta}^\top C\mathbf{q}_{-\eta}$) increases, where $\mathbf{p}_{\pm\eta} = \cos(\boldsymbol{\theta}_{\pm\eta}(k))$, $\mathbf{q}_{\pm\eta} = \sin(\boldsymbol{\theta}_{\pm\eta}(k))$ and $\boldsymbol{\theta}_{\pm\eta}(k)$ is given in (5.7).

Now, we make some assumptions about the matrix A. For convenience, we use $(\cdot)_j$ for $(\cdot)_i$, where the subscript $i \equiv j \pmod n$, if $j \notin \{1,\dots,n\}$.

Assumption 5.3. Suppose that $\hat{\boldsymbol{\theta}} = (\hat\theta_1,\dots,\hat\theta_n)^\top \in \Theta$ with $0 = \hat\theta_1 = \hat\theta_2 < \hat\theta_3 < \cdots < \hat\theta_n < 2\pi$ and for each $s \in \{1,\dots,n\}$, $\omega_{r+1}(\boldsymbol{\theta}_0) > 0$ and $\omega_r(\boldsymbol{\theta}_0) < 0$, where $\boldsymbol{\theta}_0 \equiv \boldsymbol{\theta}(s)$ in (5.6) and $r \equiv n-s+2 \pmod n$. Then, there is a $s \in \{1,\dots,n\}$ such that one of the following conditions holds

(i) there exists $k \in I_+^s$ (or $k \in I_-^s$) such that $\omega_k(\boldsymbol{\theta}_0) < 0$ (or $\omega_k(\boldsymbol{\theta}_0) > 0$); or

(ii) there exists $k \in I_+^s$ such that $0 < \omega_{r+1}(\boldsymbol{\theta}_0) < \omega_k(\boldsymbol{\theta}_0)$ and

$$1 - \cos(\theta_{r+2} - \theta_{r+1}) \geqslant \cos(\theta_k - \theta_{k-1}) - \cos(\theta_{k+1} - \theta_k);\ \text{or}$$

(iii) there exists $k \in I_-^s$ such that $0 > \omega_r(\boldsymbol{\theta}_0) > \omega_k(\boldsymbol{\theta}_0)$ and

$$1 - \cos(\theta_r - \theta_{r-1}) \geqslant \cos(\theta_{k+1} - \theta_k) - \cos(\theta_k - \theta_{k-1}).$$

In the following Remark 5.4 (a), (b) and (c), we explain that Assumption 5.3 exists generically and depends strongly on the structure of matrix A. The reader can skip this remark and go directly to Theorem 5.5.

Remark 5.4. (a) I_+^s and I_-^s in (5.10) cannot both be empty sets. If $I_+^s = I_-^s = \emptyset$, then $\bar{\mathbf{p}} = \cos(\bar{\boldsymbol{\theta}})$, $\bar{\mathbf{q}} = \sin(\bar{\boldsymbol{\theta}})$ with $\bar{\boldsymbol{\theta}} := (0, \frac{2\pi}{n}, \dots, (n-1)\frac{2\pi}{n})^\top$ must satisfy equation (3.20) and $\bar{\mathbf{p}}\cdot\bar{\mathbf{p}} + \bar{\mathbf{q}}\cdot\bar{\mathbf{q}} = \mathbf{1}$. However, the solutions of these equations, in general, form an isolated set. Thus, $\bar{\mathbf{p}}$ and $\bar{\mathbf{q}}$, generally, cannot satisfy the equation (3.20) with a general M-matrix A.

(b) For each $\hat{\boldsymbol{\theta}} = (\hat{\theta}_1, \ldots, \hat{\theta}_n)^\top \in \Theta$ with $0 = \hat{\theta}_1 = \hat{\theta}_2 < \hat{\theta}_3 < \ldots < \hat{\theta}_n < 2\pi$ and $s \in \{1, \ldots, n\}$, we set $\boldsymbol{\theta}_0 = \boldsymbol{\theta}(s) = (\theta_1, \ldots, \theta_n)^\top \in \Theta$ in (5.6). Then, we have $\theta_k \equiv \hat{\theta}_{s-1+k} - \hat{\theta}_s \pmod{2\pi}$; hence, $\boldsymbol{\theta}_0 - \theta_k \mathbf{1} = (\theta_1 - \theta_k, \ldots, \theta_n - \theta_k)^\top$, where

$$\theta_i - \theta_k \equiv \hat{\theta}_{s-1+i} - \hat{\theta}_{s-1+k} \pmod{2\pi}. \tag{5.12}$$

It follows from (5.11) that

$$\omega_k(\boldsymbol{\theta}_0) = [\sin(\hat{\theta}_s - \hat{\theta}_{s-1+k}), \sin(\hat{\theta}_{s+1} - \hat{\theta}_{s-1+k}), \ldots, \sin(\hat{\theta}_{s+n-1} - \hat{\theta}_{s-1+k})]\mathbf{a}_k. \tag{5.13}$$

Let $r \equiv n - s + 2 \pmod{n}$; it follows from (5.13) that $\omega_{r+1}(\boldsymbol{\theta}_0) > 0$, $\omega_r(\boldsymbol{\theta}_0) < 0$ can be rewritten as

$$\begin{aligned} &[\sin(\hat{\theta}_s - \hat{\theta}_2), \sin(\hat{\theta}_{s+1} - \hat{\theta}_2), \ldots, \sin(\hat{\theta}_{s+n-1} - \hat{\theta}_2)]\mathbf{a}_{n-s+3} > 0, \\ &[\sin(\hat{\theta}_s - \hat{\theta}_1), \sin(\hat{\theta}_{s+1} - \hat{\theta}_1), \ldots, \sin(\hat{\theta}_{s+n-1} - \hat{\theta}_1)]\mathbf{a}_{n-s+2} < 0. \end{aligned} \tag{5.14}$$

Let $S \in \mathbb{R}^{n\times n}$ be the permutation with

$$\begin{cases} S_{i,i+1} = S_{n,1} = 1, \\ 0, \text{ otherwise}, \end{cases} \quad \text{and } \Phi = \left[(S^\top)^n \mathbf{a}_1, (S^\top)^{n-1}\mathbf{a}_2, \cdots, S^\top \mathbf{a}_n\right]. \tag{5.15}$$

Here, Φ is dependent on only matrix A. Since $\hat{\theta}_1 = \hat{\theta}_2 = 0$, (5.14) becomes

$$\begin{bmatrix} -\Phi^\top \\ \Phi^\top S \end{bmatrix} \sin\hat{\boldsymbol{\theta}} > \mathbf{0}. \tag{5.16}$$

Note that (5.16) shows that there is a hyperplane with normal vector $\sin\hat{\boldsymbol{\theta}}$ such that the $2n$ column vectors of $[-\Phi, S^\top\Phi]$ lie in the halfspace determined by this plane. Assumption 5.3 states that if there is a $\hat{\boldsymbol{\theta}} \in \Theta$ with $0 = \hat{\theta}_1 = \hat{\theta}_2$ such that (5.16) holds, then we need one of the additional conditions (i), (ii), or (iii).

(c) Suppose that $\hat{\boldsymbol{\theta}} = (\hat{\theta}_1, \ldots, \hat{\theta}_n)^\top \in \Theta$ with $0 = \hat{\theta}_1 = \hat{\theta}_2 < \hat{\theta}_3 < \ldots < \hat{\theta}_n < 2\pi$. For $\ell \in \{3, 4, \ldots, n\}$, we set $\hat{\theta}_{n+1} = 0$ and define

$$I_+ = \left\{ \ell \mid \hat{\theta}_\ell < \frac{\hat{\theta}_{\ell-1} + \hat{\theta}_{\ell+1}}{2} \right\}, \; I_- = \left\{ \ell \mid \hat{\theta}_\ell > \frac{\hat{\theta}_{\ell-1} + \hat{\theta}_{\ell+1}}{2} \right\}, \tag{5.17}$$

From the vector $\boldsymbol{\theta}(s)$ in (5.6), we have $\theta_{\ell-s+1} \equiv \hat{\theta}_\ell - \hat{\theta}_s \pmod{2\pi}$; hence,

$$I_\pm^s = I_\pm - (s-1) := \{\ell - s + 1 \mid \ell \in I_\pm\}_{\mathrm{mod}_n}, \tag{5.18}$$

where $I_\pm^s$ is defined in (5.10). According to (5.13), (5.14), and matrix S in (5.15), those three additional conditions in Assumption 5.3 can be rewritten as for some $s \in \{1, \ldots, n\}$,

(i) there exists $\ell \in I_+$ (or $\ell \in I_-$) such that

$$\mathbf{a}_{\ell-s+1}^\top S^{s-1} \sin(\hat{\boldsymbol{\theta}} - \hat{\theta}_\ell \mathbf{1}) < 0 \text{ (or } \mathbf{a}_{\ell-s+1}^\top S^{s-1} \sin(\hat{\boldsymbol{\theta}} - \hat{\theta}_\ell \mathbf{1}) > 0).$$

(ii) there exists $\ell \in I_+$ such that

$$0 < \mathbf{a}_{n-s+3}^\top S^{s-1} \sin \hat{\boldsymbol{\theta}} < \mathbf{a}_{\ell-s+1}^\top S^{s-1} \sin(\hat{\boldsymbol{\theta}} - \hat{\theta}_\ell \mathbf{1}) \text{ and}$$
$$1 - \cos \hat{\theta}_3 \geqslant \cos(\hat{\theta}_\ell - \hat{\theta}_{\ell-1}) - \cos(\hat{\theta}_{\ell+1} - \hat{\theta}_\ell).$$

(iii) there exists $\ell \in I_-$ such that

$$0 > \mathbf{a}_{n-s+2}^\top S^{s-1} \sin \hat{\boldsymbol{\theta}} > \mathbf{a}_{\ell-s+1}^\top S^{s-1} \sin(\hat{\boldsymbol{\theta}} - \hat{\theta}_\ell \mathbf{1}) \text{ and}$$
$$1 - \cos \hat{\theta}_n \geqslant \cos(\hat{\theta}_{\ell+1} - \hat{\theta}_\ell) - \cos(\hat{\theta}_\ell - \hat{\theta}_{\ell-1}).$$

Theorem 5.5. *Assume that the CEM problem in (5.2) has a nontrivial local minimizer $\boldsymbol{\theta} \in \Theta$ and Assumption 5.3 holds. Then, $\boldsymbol{\theta}$ has distinct angle partitions.*

Proof. We prove the assertion by contradiction. Without loss of generality, we suppose that $\hat{\boldsymbol{\theta}} = (\hat{\theta}_1, \ldots, \hat{\theta}_n)^\top \in \Theta$ with $0 = \hat{\theta}_1 = \hat{\theta}_2 < \hat{\theta}_3 < \ldots < \hat{\theta}_n < 2\pi$ is a nontrivial local minimum. Since any rotation of $\hat{\boldsymbol{\theta}}$ by a constant is also a local minimal solution of $E_C(\boldsymbol{\theta}; \beta)$, for any fixed $s \in \{1, \ldots, n\}$, $\boldsymbol{\theta}_0 \equiv \boldsymbol{\theta}(s) = (\theta_1, \ldots, \theta_r, \theta_{r+1}, \ldots, \theta_n)^\top \in \Theta$ in (5.6) is also a local minimum. Note that $\theta_r = \theta_{r+1}$ and $r \equiv n - s + 2 \pmod n$.

We now consider the perturbation of angles at θ_{r+1} (or θ_r) with sufficiently small $\eta > 0$ (or $-\eta < 0$), i.e., $\boldsymbol{\theta}_\eta(r+1)$ (or $\boldsymbol{\theta}_{-\eta}(r)$), as in (5.7), and denote

$$\boldsymbol{\theta}_\eta \equiv \boldsymbol{\theta}_\eta(r+1) \text{ and } \boldsymbol{\theta}_{-\eta} \equiv \boldsymbol{\theta}_{-\eta}(r). \tag{5.19}$$

Let

$$\mathbf{p}_{\pm\eta} = \cos(\boldsymbol{\theta}_{\pm\eta}) \text{ and } \mathbf{q}_{\pm\eta} = \sin(\boldsymbol{\theta}_{\pm\eta}). \tag{5.20}$$

Using the fact that $\theta_r = \theta_{r+1}$, it follows from (5.8b) of Lemma 5.2 that

$$\mathbf{p}_{\pm\eta}^\top C \mathbf{q}_{\pm\eta} - \mathbf{p}_0^\top C \mathbf{q}_0 = c_\pm \eta + O(\eta^2), \tag{5.21}$$

where $c_+ = 1 - \cos(\theta_{r+2} - \theta_{r+1}) > 0$ and $c_- = 1 - \cos(\theta_r - \theta_{r-1}) > 0$.

Plugging $\mathbf{p}_{\pm\eta}$, $\mathbf{q}_{\pm\eta}$ in (5.20) into $E_C(\boldsymbol{\theta}_{\pm\eta}; \beta)$, from (5.21) and (5.8a) of Lemma 5.2, we have

$$\begin{aligned} E_C(\boldsymbol{\theta}_\eta; \beta) =& \frac{1}{2}\mathbf{p}_\eta^\top A \mathbf{p}_\eta + \frac{1}{2}\mathbf{q}_\eta^\top A \mathbf{q}_\eta - \frac{\beta}{2}\mathbf{p}_\eta^\top C \mathbf{q}_\eta \\ =& \frac{1}{2}(\mathbf{p}_0^\top A \mathbf{p}_0 + \mathbf{q}_0^\top A \mathbf{q}_0 - \beta \mathbf{p}_0^\top C \mathbf{q}_0) + \eta \omega_{r+1}(\boldsymbol{\theta}_0) - \frac{\beta c_+}{2}\eta + O(\eta^2); \end{aligned} \tag{5.22a}$$

or

$$\begin{aligned} E_C(\boldsymbol{\theta}_{-\eta}; \beta) =& \frac{1}{2}\mathbf{p}_{-\eta}^\top A \mathbf{p}_{-\eta} + \frac{1}{2}\mathbf{q}_{-\eta}^\top A \mathbf{q}_{-\eta} - \frac{\beta}{2}\mathbf{p}_{-\eta}^\top C \mathbf{q}_{-\eta} \\ =& \frac{1}{2}(\mathbf{p}_0^\top A \mathbf{p}_0 + \mathbf{q}_0^\top A \mathbf{q}_0 - \beta \mathbf{p}_0^\top C \mathbf{q}_0) - \eta \omega_r(\boldsymbol{\theta}_0) - \frac{\beta c_-}{2}\eta + O(\eta^2), \end{aligned} \tag{5.22b}$$

where $\omega_{r+1}(\boldsymbol{\theta}_0)$, $\omega_r(\boldsymbol{\theta}_0)$ are defined in (5.11) and $c_\pm > 0$ are given in (5.21). Next, we consider the following cases.

Case I. There is an $s \in \{1, \dots, n\}$ such that $\omega_{r+1}(\boldsymbol{\theta}_0) \leqslant 0$ (or $\omega_r(\boldsymbol{\theta}_0) \geqslant 0$):
It follows from (5.22) that

$$E_C(\boldsymbol{\theta}_\eta; \beta) = E_C(\boldsymbol{\theta}_0; \beta) - c\eta + O(\eta^2) \text{ with } c = -\omega_{r+1}(\boldsymbol{\theta}_0) + \beta c_+/2 > 0$$
$$\text{or } E_C(\boldsymbol{\theta}_{-\eta}; \beta) = E_C(\boldsymbol{\theta}_0; \beta) - c\eta + O(\eta^2) \text{ with } c = \omega_r(\boldsymbol{\theta}_0) + \beta c_-/2 > 0.$$

For sufficiently small $\eta > 0$, we have $E_C(\boldsymbol{\theta}_\eta; \beta) < E_C(\boldsymbol{\theta}_0; \beta)$ (or $E_C(\boldsymbol{\theta}_{-\eta}; \beta) < E_C(\boldsymbol{\theta}_0; \beta)$), which is contradictory to stating that $\boldsymbol{\theta}_0$ is a local minimum for $E_C(\boldsymbol{\theta}; \beta)$.

Case II. Suppose that for each $s \in \{1, \dots, n\}$, we have $\omega_{r+1}(\boldsymbol{\theta}_0) > 0$ and $\omega_r(\boldsymbol{\theta}_0) < 0$:
We now consider two perturbations of angles at $\theta_r = \theta_{r+1}$ and θ_k, with sufficiently small $\eta > 0$ and $|\xi_k| = O(\eta)$, to be determined as

$$\boldsymbol{\theta}_\eta \equiv \boldsymbol{\theta}_\eta(r+1, k) = (\theta_1, \dots, \theta_{r-1}, \theta_r, \theta_r + \eta, \dots, \theta_k + \xi_k, \dots, \theta_n)^\top, \tag{5.23a}$$
$$\boldsymbol{\theta}_{-\eta} \equiv \boldsymbol{\theta}_{-\eta}(r, k) = (\theta_1, \dots, \theta_{r-1}, \theta_r - \eta, \theta_r, \dots, \theta_k + \xi_k, \dots, \theta_n)^\top. \tag{5.23b}$$

Let $\mathbf{p}_{\pm\eta} = \cos(\boldsymbol{\theta}_{\pm\eta})$ and $\mathbf{q}_{\pm\eta} = \sin(\boldsymbol{\theta}_{\pm\eta})$. By plugging $\mathbf{p}_{\pm\eta}$, $\mathbf{q}_{\pm\eta}$ into $E_C(\boldsymbol{\theta}_{\pm\eta}; \beta)$, it follows from Lemma 5.2 that

$$\begin{aligned} E_C(\boldsymbol{\theta}_\eta; \beta) =& \frac{1}{2}\mathbf{p}_\eta^\top A \mathbf{p}_\eta + \frac{1}{2}\mathbf{q}_\eta^\top A \mathbf{q}_\eta - \frac{\beta}{2}\mathbf{p}_\eta^\top C \mathbf{q}_\eta \\ =& \frac{1}{2}(\mathbf{p}_0^\top A \mathbf{p}_0 + \mathbf{q}_0^\top A \mathbf{q}_0 - \beta \mathbf{p}_0^\top C \mathbf{q}_0) + \eta\omega_{r+1}(\boldsymbol{\theta}_0) + \xi_k \omega_k(\boldsymbol{\theta}_0) \\ & - (\frac{\beta c_+}{2}\eta + O(\xi_k)) + O(\eta^2 + \xi_k^2); \end{aligned} \tag{5.24a}$$

or

$$\begin{aligned} E_C(\boldsymbol{\theta}_{-\eta}; \beta) =& \frac{1}{2}\mathbf{p}_{-\eta}^\top A \mathbf{p}_{-\eta} + \frac{1}{2}\mathbf{q}_{-\eta}^\top A \mathbf{q}_{-\eta} - \frac{\beta}{2}\mathbf{p}_{-\eta}^\top C \mathbf{q}_{-\eta} \\ =& \frac{1}{2}(\mathbf{p}_0^\top A \mathbf{p}_0 + \mathbf{q}_0^\top A \mathbf{q}_0 - \beta \mathbf{p}_0^\top C \mathbf{q}_0) - \eta\omega_r(\boldsymbol{\theta}_0) + \xi_k \omega_k(\boldsymbol{\theta}_0) \\ & - (\frac{\beta c_-}{2}\eta + O(\xi_k)) + O(\eta^2 + \xi_k^2), \end{aligned} \tag{5.24b}$$

where $\omega_r(\boldsymbol{\theta}_0), \omega_{r+1}(\boldsymbol{\theta}_0), \omega_k(\boldsymbol{\theta}_0)$ are defined in (5.11) and $c_\pm > 0$ are defined in (5.21).

(i) Assume that Assumption 5.3 (i) holds:
Suppose that there is a $k \in I_+^s$ such that $\omega_k(\boldsymbol{\theta}_0) < 0$. Since $k \in I_+^s$, we need to choose $\xi_k > 0$ to increase the area of the perturbed polygon. Under the condition that $\omega_{r+1}(\boldsymbol{\theta}_0) > 0$, $\xi_k = O(\eta) > 0$ can be solved by $\eta\omega_{r+1}(\boldsymbol{\theta}_0) + \xi_k\omega_k(\boldsymbol{\theta}_0) = 0$, as in (5.24a), to make it zero. Thus, for sufficiently small $\eta > 0$, it follows from (5.24a) that $E_C(\boldsymbol{\theta}_\eta; \beta) < E_C(\boldsymbol{\theta}_0; \beta)$. This is a contradiction.
Similarly, if there is a $k \in I_-^s$ such that $\omega_k(\boldsymbol{\theta}_0) > 0$, a $\xi_k < 0$ must be chosen to increase the size of the perturbed polygon. Using the condition that $\omega_r(\boldsymbol{\theta}_0) < 0$, $\xi_k = O(\eta) < 0$ can be solved by $-\eta\omega_r(\boldsymbol{\theta}_0) + \xi_k\omega_k(\boldsymbol{\theta}_0) = 0$, as in (5.24b). It follows from (5.24b) that $E_C(\boldsymbol{\theta}_{-\eta}; \beta) < E_C(\boldsymbol{\theta}_0; \beta)$. This is also a contradiction.

(ii) Assume that Assumption 5.3 (ii) holds:
Suppose that there are $s \in \{1, \ldots, n\}$ and $k \in I_+^s$ such that $0 < \omega_{r+1}(\boldsymbol{\theta}_0) < \omega_k(\boldsymbol{\theta}_0)$. We consider $\xi_k = -\eta$ in (5.23a); then,

$$\begin{aligned} \mathbf{p}_\eta &= \cos(\boldsymbol{\theta}_0) - \eta \sin\theta_r \mathbf{e}_{r+1} + \eta \sin\theta_k \mathbf{e}_k, \\ \mathbf{q}_\eta &= \sin(\boldsymbol{\theta}_0) + \eta \cos\theta_r \mathbf{e}_{r+1} - \eta \cos\theta_k \mathbf{e}_k. \end{aligned}$$

Since $\mathbf{p}_0 = \cos(\boldsymbol{\theta}_0)$, $\mathbf{q}_0 = \sin(\boldsymbol{\theta}_0)$ and $\theta_r = \theta_{r+1}$, it follows from Lemma 5.2 that

$$\mathbf{p}_\eta^\top C \mathbf{q}_\eta = \mathbf{p}_0^\top C \mathbf{q}_0 + \eta\rho_k + O(\eta^2),$$

where $\rho_k = 1 - \cos(\theta_{r+2} - \theta_{r+1}) + \cos(\theta_{k+1} - \theta_k) - \cos(\theta_k - \theta_{k-1}) \geqslant 0$, as in Assumption 5.3 (ii). Then, equation (5.24a) becomes

$$E_C(\boldsymbol{\theta}_\eta; \beta) = E_C(\boldsymbol{\theta}_0; \beta) + \eta(\omega_{r+1}(\boldsymbol{\theta}_0) - \omega_k(\boldsymbol{\theta}_0)) - \frac{\beta}{2}\rho_k\eta + O(\eta^2). \tag{5.25}$$

Since $\omega_{r+1}(\boldsymbol{\theta}_0) - \omega_k(\boldsymbol{\theta}_0) < 0$ and $\rho_k \geqslant 0$, from (5.25), we have $E_C(\boldsymbol{\theta}_\eta; \beta) < E_C(\boldsymbol{\theta}_0; \beta)$. This is a contradiction.

(iii) Assume that Assumption 5.3 (iii) holds:
We also obtain a contradiction for this case, and the proof is similar to the proof in (ii).

We prove that under assumption Assumption 5.3, the local minimum of $E_C(\boldsymbol{\theta}; \beta)$ must have distinct angle partitions. ∎

Theorem 5.6. *Assume that Assumption 5.3 holds. There exists $\hat{\beta} > 0$ such that the CEM problem with $\beta > \hat{\beta}$ in (5.2) has a local minimizer $\boldsymbol{\theta} \in \Theta$ with all partition angles being distinct.*

Proof. Let $\bar{\boldsymbol{\theta}}$, $\bar{\mathbf{p}}$ and $\bar{\mathbf{q}}$ be defined as in Remark 5.4 (a). From (3.11), it follows that

$$\bar{\mathbf{p}}^\top C \bar{\mathbf{q}} = \sum_{j=1}^{n} \sin(\theta_{j+1} - \theta_j) = n \sin\left(\frac{2\pi}{n}\right) > 0. \tag{5.26}$$

Using the definition of $E_C(\boldsymbol{\theta}; \beta)$ in (5.1), we have $h(\beta) < 0$ for some sufficiently large β. Lemma 5.1 shows that $\boldsymbol{\theta} = \mathbf{0}$ is the global minimizer of (5.2) and $h(\beta) = E_C(\mathbf{0}; \beta) = 0$ for sufficiently small β . Hence, there exists a $\beta_0 > 0$ such that

$$h(\beta) = \begin{cases} 0, & \text{if } \beta \leqslant \beta_0, \\ < 0, & \text{if } \beta > \beta_0. \end{cases} \tag{5.27}$$

Lemma 5.1 also shows that the trivial state $\boldsymbol{\theta} = \mathbf{0}$ is a strict local minimizer of (5.2) with energy $E_C(\mathbf{0}; \beta) = 0$ for all $\beta > 0$. From (5.27), it follows that there is a nontrivial global minimizer $\boldsymbol{\theta}_{\beta_0} \in \Theta$ of (5.2) with $h(\beta_0) = E_C(\boldsymbol{\theta}_{\beta_0}; \beta_0) = 0$. According to Theorem 5.5, the nontrivial minimizer $\boldsymbol{\theta}_{\beta_0}$ has a distinct angle partition. This result implies that $E_C(\boldsymbol{\theta}; \beta_0)$ forms a double well function having two local minima and bifurcated at $\beta = \beta_0$.

Since $\boldsymbol{\theta} = \mathbf{0}$ is a strict local minimizer of (5.2) with $\beta = \beta_0$, there is a $\delta_0 > 0$ with $\delta_0 < \|\boldsymbol{\theta}_{\beta_0}\|_2$ such that $E_C(\boldsymbol{\theta}; \beta_0) > 0$ for $\boldsymbol{\theta} \in \Theta_{\delta_0} := \Theta \cap \{\boldsymbol{\theta} \in \mathbb{R}^n \mid \|\boldsymbol{\theta}\|_2 = \delta_0\}$. Let

$$\varepsilon_0 = \min_{\boldsymbol{\theta} \in \Theta_{\delta_0}} E_C(\boldsymbol{\theta}; \beta_0) > 0.$$

Denote $\Theta_{\geqslant \delta_0} := \Theta \cap \{\boldsymbol{\theta} \in \mathbb{R}^n \mid \|\boldsymbol{\theta}\|_2 \geqslant \delta_0\}$ and let $cl(\Theta_{\geqslant \delta_0})$ be the closure of $\Theta_{\geqslant \delta_0}$. Then, $\boldsymbol{\theta}_{\beta_0} \in \Theta_{\geqslant \delta_0}$. Since $cl(\Theta_{\geqslant \delta_0})$ is compact and $E_C(\boldsymbol{\theta}_{\beta_0}; \beta_0) = 0 < \varepsilon_0$, there exists a positive number $\hat{\beta} < \beta_0$ such that for each $\beta \in (\hat{\beta}, \beta_0]$ the CEM problem in (5.2) has a nontrivial local minimizer $\boldsymbol{\theta}_\beta \in cl(\Theta_{\geqslant \delta_0})$ and $0 \leqslant E_C(\boldsymbol{\theta}_\beta; \beta) < \varepsilon_0$. For the parameter $\beta > \beta_0$, since $E_C(\boldsymbol{\theta}; \beta)$ is continuous, $cl(\Theta)$ is compact, and $h(\beta) < 0$, $E_C(\boldsymbol{\theta}; \beta)$ has a nontrivial local minimizer $\boldsymbol{\theta}_\beta \in cl(\Theta)$ and $h(\beta) = E_C(\boldsymbol{\theta}_\beta; \beta) < 0$. Applying Theorem 5.5, the nontrivial minimizer $\boldsymbol{\theta}_\beta \in \Theta$ has a distinct angle partition for $\beta > \hat{\beta}$. ∎

Remark 5.7. The conformal energy $E_C(\boldsymbol{\theta})$ in (3.17) is the energy function $E_C(\boldsymbol{\theta}, \beta)$ in (5.1) with $\beta = 1$. Theorem 5.6 shows that if $1 > \hat{\beta}$, then the CEM problem in (3.18) has a local minimizer with a distinct angle partition. In this case, Theorem 4.1 shows that Algorithm 3.1 proposed in this paper converges globally.

6. Numerical experiments. In this section, we present numerical results of the proposed CCEM algorithm for the computation of disk-shaped conformal parameterizations of several benchmark mesh models. All experiments are performed in MATLAB on a personal computer with a 3.60 GHz CPU and 32 GB RAM. The triangular mesh models are obtained from the AIM@SHAPE shape repository [1], the Stanford 3D scanning repository [2], and Sketchfab [3]. Some of the mesh models are resampled or modified such that no triangle is composed of merely boundary vertices.

In the following experiments, the initial map is computed by the previous CEM algorithm [38] with a maximum number of iterations of 20 and a tolerance for energy differences of 10^{-6}. To address efficiency concerns, the maximum number of iterations of the CCEM algorithm is set to 20 and the tolerance for energy differences is 10^{-7}.

In Figure 1, we show the circle patterns mapped from the image of parameterizations to the models *Buddha* and *Max Planck* by the inverse map of the disk conformal parameterizations computed by the CCEM algorithms. The circle patterns are well-preserved, which means the parameterization is conformal.

In Figure 2, we show the disk-shaped conformal parameterizations of the mesh models *Human Brain*, *David Head*, *Buddha* and *Nefertiti Statue* computed by the CCEM algorithm. The histograms of their angular distortions are also illustrated. Most of the angular distortions are less than 5 degrees, even when the shape of the surface is complicated, as for *Human Brain*, which is satisfactory.

6.1. Convergence behavior. To illustrate the convergence behavior of the gradient descent iterations with the quadratic approximation in the proposed CCEM algorithm, we set the number of iterations to 100. In Figure 3, we show the relationship between the number of iterations and the conformal energy of the mappings for the mesh models *Cat Face*, *Human Brain*, *Left Hand*, *Stanford Bunny*, *Femur*, and *Nefertiti Statue*. In Figure 3 (b), we observe a substantial drop in energy in the 73rd iteration. Apparently, this step of gradient descent

Figure 1. *The circle patterns mapped from the disk to the models* Buddha *and* Max Planck *by the inverse map of the conformal parameterization computed by the CCEM algorithms.*

shifts from a saddle point to another potential local minimizer with considerably lower conformal energy. Similar phenomena occur at the 36th and 60th iterations in Figure 3 (f). Notably, in all the tested mesh models, the conformal energy strictly decreases as the number of iterations increases, which indicates the proposed CCEM algorithm is effective in decreasing the conformal energy. Moreover, the resulting conformal mappings for the demonstrated mesh models are bijective.

6.2. Comparison with state-of-the-art algorithms. In this subsection, we compare the effectiveness and accuracy of the proposed CCEM algorithm with those of two state-of-the-art CPU-based algorithms for computing disk-shaped conformal parameterizations: the FDCP [11] and the LDCP [9]. The MATLAB programs of FDCP and LDCP are obtained from Choi's website [4]. The maximal number of iterations of the CCEM algorithm is set to 20. Moreover, the iteration process is terminated when the difference between the conformal energies of two consecutive iteration steps is less than 10^{-7}.

The conformal energy of the mappings produced by the FDCP, LDCP, and CCEM algorithms and their computational time costs are presented in Table 1. To ensure a fair comparison, the time cost of the CCEM algorithm includes the computation of the initial mapping by the CEM algorithm [38] and the line-search gradient descent with a quadratic approximation. For the models with a larger number of vertices, the initial map computed by the previous CEM algorithm [38] is already sufficiently satisfactory such that the difference between the conformal energies of the initial and first iteration step is less than 10^{-7}. For better visualization of these data, we present the conformal energy and the computational time costs in Figure 4. In Figure 4 (a), we see that among all the tested mesh models, the conformal parameterizations of the CCEM algorithm have the best, or near the best, con-

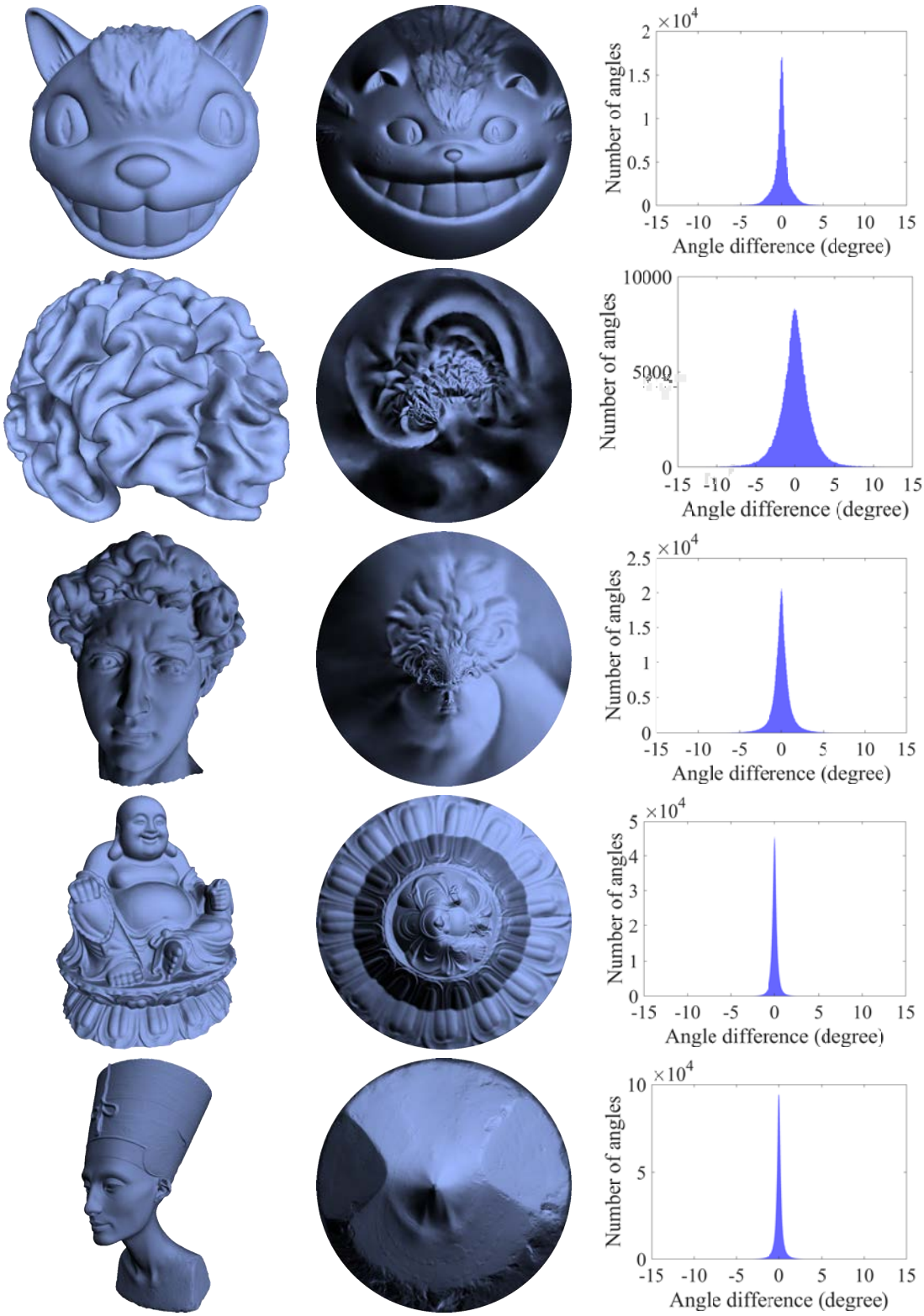

Figure 2. *The disk-shaped conformal parameterizations of the mesh models* Cat Face, Human Brain, David Head, Buddha *and* Nefertiti Statue *computed by the CCEM algorithm and the histograms of their angular distortions.*

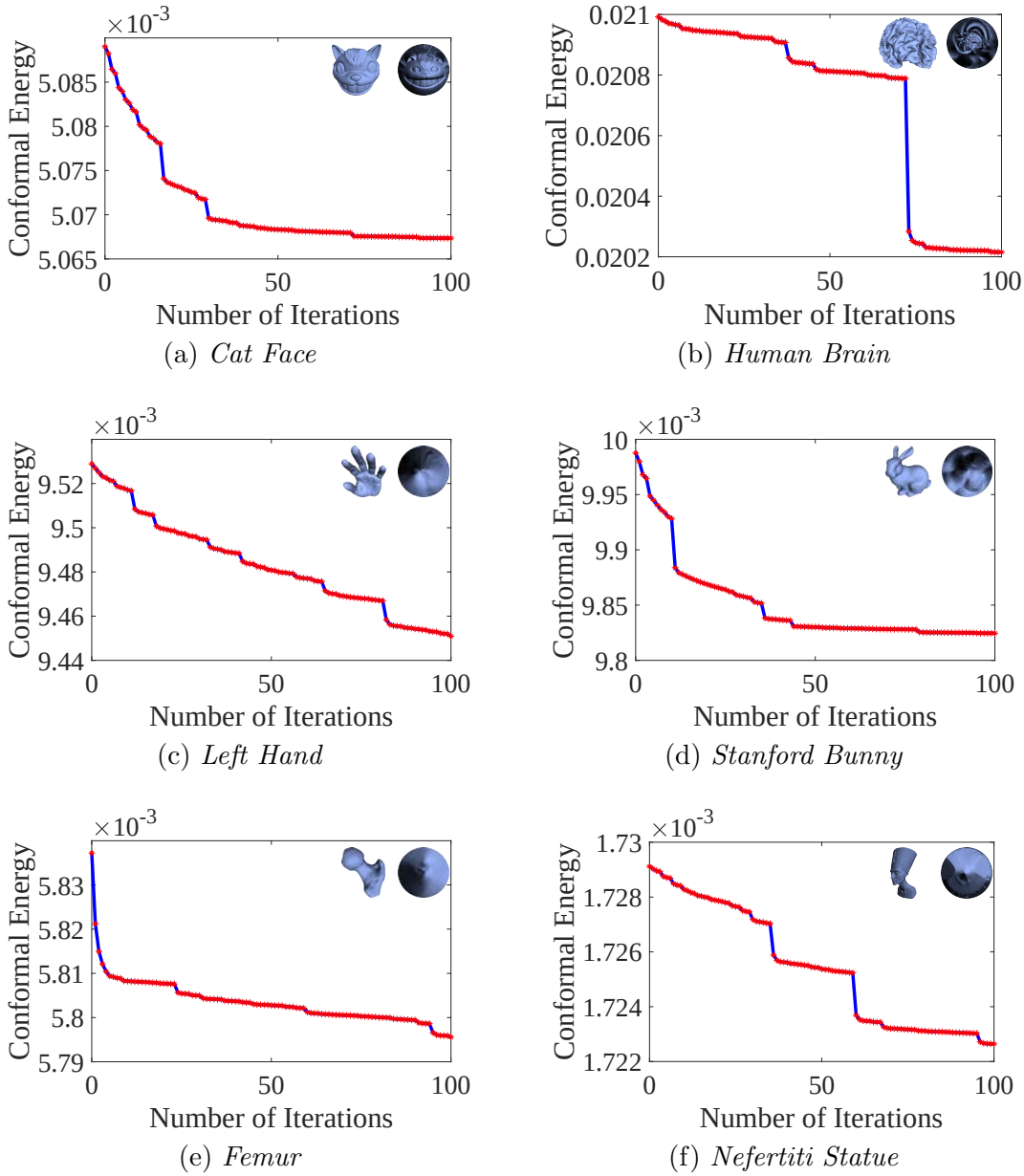

Figure 3. *The relationship between the number of iterations and the conformal energy of the parameterization obtained by the CCEM algorithm for (a)* Cat Face*, (b)* Human Brain*, (c)* Left Hand*, (d)* Stanford Bunny*, (e)* Femur*, and (f)* Nefertiti Statue*.*

formality in terms of conformal energy. From Figure 4 (b), we see that the efficiency of the CCEM algorithm is similar to that of the LDCP and significantly better than that of the FDCP.

In addition, in Figure 5, we present the mean and standard deviation (SD) of the moduli of angular distortions (in degrees). The angular distortion is the difference between the angles

Table 1

The computational time cost (sec.) and conformal energy of conformal parameterizations by the FDCP [11], LDCP [9], and CCEM algorithms. The maximum number of iterations of the CCEM algorithm is 20*, and the tolerance for energy differences is* 10^{-7}*. The time cost of the CCEM algorithm includes the computation of the initial mapping by the CEM algorithm [38] and the line-search gradient descent with a quadratic approximation.*

Model	#Vertices	FDCP [11]		LDCP [9]		CCEM		
		E_C	Time	E_C	Time	E_C	Time	#Iter.
Ear	367	0.1653	0.03	0.2079	0.01	0.1415	0.01	20
Bourbon Bottle	6,569	0.0110	0.26	0.0110	0.13	0.0110	0.07	2
Foot	10,010	0.0128	0.35	0.0164	0.23	0.0113	0.22	20
Chinese Lion	17,334	0.0139	1.32	0.0141	0.47	0.0139	0.35	15
Femur	21,699	0.0058	1.51	0.0058	0.63	0.0058	0.42	8
Hat	22,118	0.0001	2.18	0.0001	0.75	0.0001	0.51	9
Stanford Bunny	31,593	0.0104	2.26	0.0100	0.94	0.0100	1.06	20
Cat Face	33,185	0.0052	2.89	0.0054	1.06	0.0051	0.92	20
Max Planck	41,588	0.0082	2.46	0.0079	1.28	0.0079	1.52	20
Human Brain	48,463	0.0213	3.48	0.0244	1.44	0.0209	1.57	20
Left Hand	53,011	0.0098	6.60	0.0094	1.98	0.0095	1.72	20
Knit Cap Man	59,561	0.0059	8.04	0.0061	2.47	0.0058	1.89	17
David Head	101,146	0.0044	14.36	0.0045	4.93	0.0044	4.35	20
Bimba Statue	216,873	0.0010	43.54	0.0011	12.59	0.0010	4.41	1
Buddha	473,362	0.0007	87.88	0.0007	30.74	0.0007	11.56	1
Nefertiti Statue	996,838	0.0017	212.45	0.0042	58.69	0.0017	19.74	1

on the triangular mesh model and that on the image. Furthermore, in Figure 6, we present the mean and SD of the moduli of the Beltrami coefficients [28]: a conformal map has zero Beltrami coefficients [28]. We observe that the conformality distortions in terms of both angular distortion moduli and Beltrami coefficient moduli are consistent with the conformal energy. In summary, under the above three classical conformality measurements, the CCEM algorithm has the best, or near the best, conformality.

Furthermore, the relationship between the number of vertices and the computational time cost is illustrated in Figure 7. As the number of vertices increases, the computational time cost increases rapidly for the FDCP, increases approximately linearly for the LDCP, and does not increase substantially for the CCEM algorithm. This result indicates that the proposed CCEM algorithm is significantly more efficient than the FDCP and LDCP, so it is suitable for the computation of conformal parameterizations of mesh models with extremely large numbers of vertices.

In summary, compared to the state-of-the-art algorithms FDCP and LDCP, the proposed CCEM algorithm has competitive accuracy and significantly better efficiency.

6.3. Efficiency of the CCEM Algorithm. The computational time cost of the CCEM algorithm is dominated by the cost of the Cholesky decomposition

$$R^\top R = P^\top L_{\mathtt{I},\mathtt{I}} P, \tag{6.1}$$

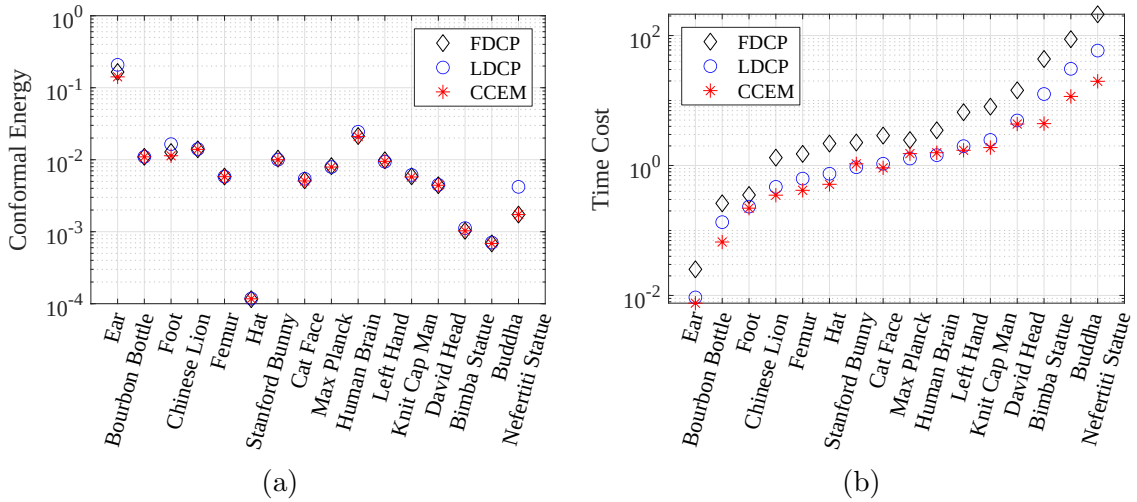

Figure 4. *The (a) conformal energy of the conformal parameterization by the FDCP, LDCP, and CCEM algorithms, and (b) their computational time costs (sec.).*

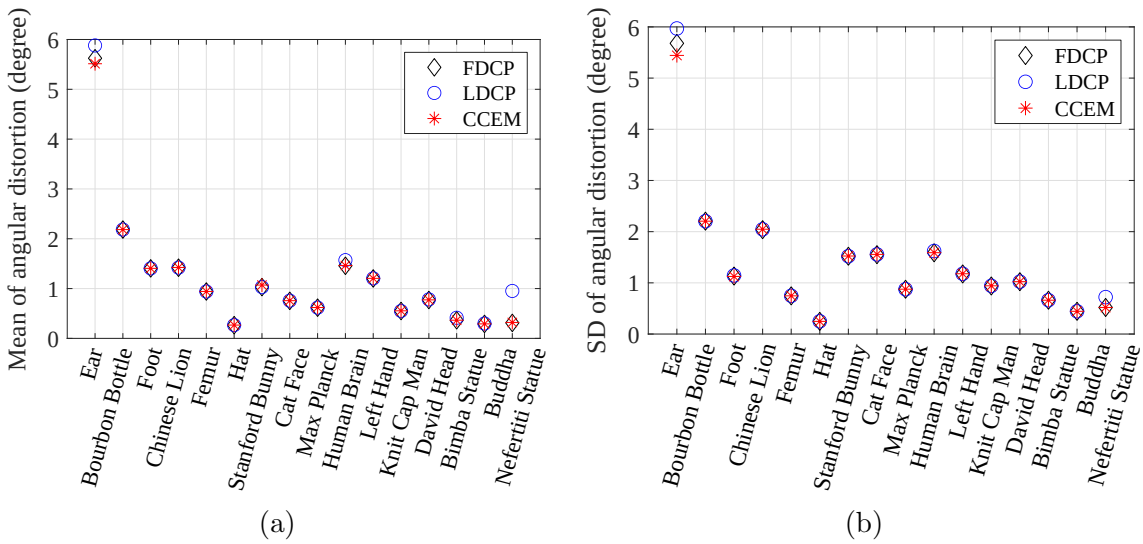

Figure 5. *The (a) mean and (b) SD of the angular distortions (in degrees) of the conformal parameterization by the FDCP, LDCP, and CCEM algorithms.*

where R is an upper triangular matrix and P is a permutation matrix. Linear systems of the form $L_{\mathtt{I},\mathtt{I}}\mathbf{x} = \mathbf{b}$ are efficiently solved by the backward substitutions $R^\top \mathbf{y} = P^\top \mathbf{b}$, $R\mathbf{z} = \mathbf{y}$, and $\mathbf{x} = P\mathbf{z}$. In practice, we compute the Cholesky decomposition (6.1) when computing the initial map via the CEM algorithm [38]. Then, we reuse the decomposition for the matrix product of A in (3.15) when performing the line-search gradient descent method with a quadratic approximation so that the additional computational time cost is relatively small. Specifically, for a triangular mesh model of roughly 1 million vertices, a conformal parameterization can be computed by the proposed CCEM algorithm in 20 seconds with

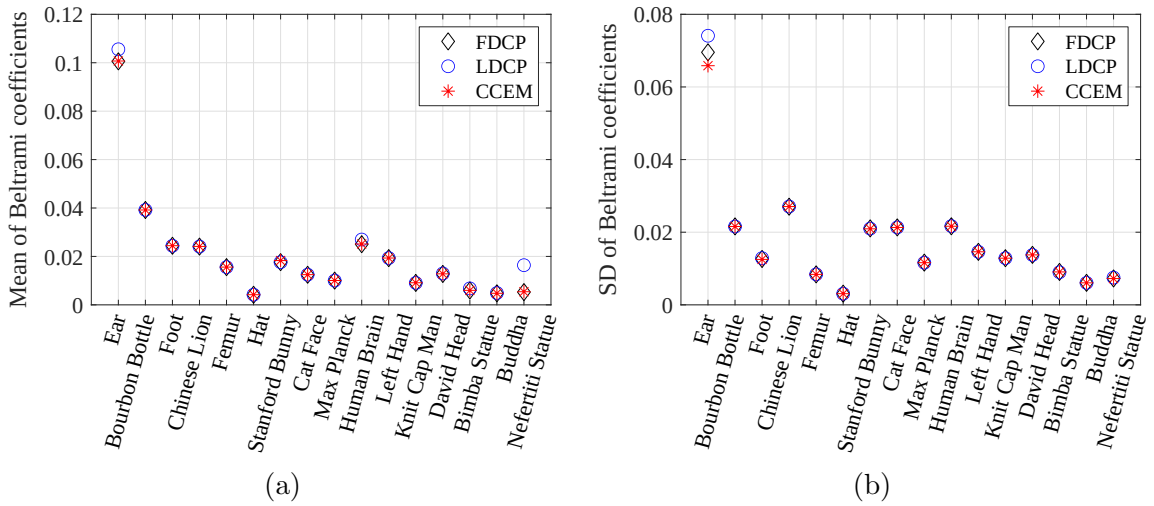

Figure 6. *The (a) mean and (b) SD of the moduli of the Beltrami coefficients of the conformal parameterization by the FDCP, LDCP, and CCEM algorithms.*

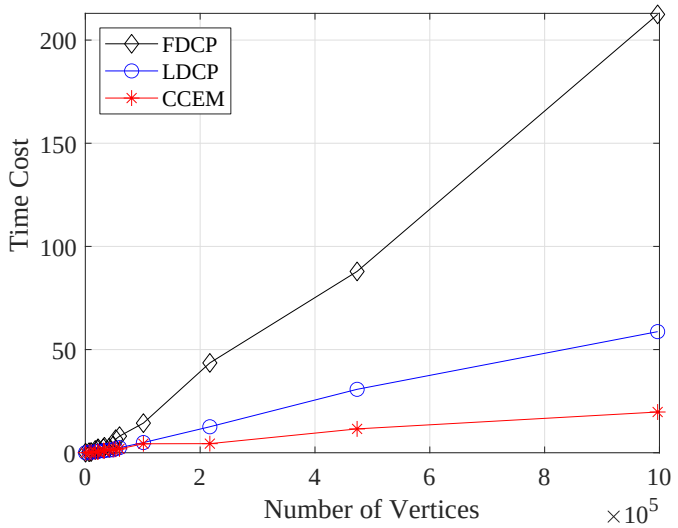

Figure 7. *The relationship between the numbers of vertices and the computational time costs for the conformal parameterization by the FDCP, LDCP, and CCEM algorithms.*

an average angular distortion of 0.32, which is satisfactory. A demonstration of MATLAB executables of the CCEM algorithm can be obtained at http://tiny.cc/DiskCCEM.

7. Concluding remarks. In this paper, we have developed a CCEM algorithm via line-search gradient descent with a quadratic approximation to compute disk-shaped conformal parameterizations of simply connected open triangular meshes. The global convergence of the CCEM algorithm is theoretically guaranteed. Additionally, the existence of the nontrivial local minimum of the CEM with bijective boundary map is guaranteed under some mild

assumptions.

Numerical experiments indicate that the CCEM algorithm has competitive accuracy and highly improved efficiency compared to state-of-the-art algorithms. Such encouraging results indicate that the CCEM algorithm is promising for real-time conformal parameterization applications.

REFERENCES

[1] *Digital Shape Workbench - Shape Repository*. http://visionair.ge.imati.cnr.it/ontologies/shapes/. (2016).

[2] *The Stanford 3D Scanning Repository*. http://graphics.stanford.edu/data/3Dscanrep/. (2016).

[3] *Sketchfab*. https://sketchfab.com/, (2019).

[4] *Gary P. T. Choi*. https://math.mit.edu/~ptchoi, (2021).

[5] P. Alliez, G. Ucelli, C. Gotsman, and M. Attene, *Recent Advances in Remeshing of Surfaces*, Springer Berlin Heidelberg, Berlin, Heidelberg, 2008, pp. 53–82, https://doi.org/10.1007/978-3-540-33265-7_2.

[6] S. Angenent, S. Haker, A. Tannenbaum, and R. Kikinis, *On the Laplace-Beltrami operator and brain surface flattening*, IEEE Trans. Med. Imaging, 18 (1999), pp. 700–711, https://doi.org/10.1109/42.796283.

[7] J.-F. Bonnans, J. C. Gilbert, C. Lemaréchal, and C. A. Sagastizábal, *Numerical optimization: theoretical and practical aspects*, Springer Science & Business Media, 2006.

[8] G. P. T. Choi, Y. Leung-Liu, X. Gu, and L. M. Lui, *Parallelizable global conformal parameterization of simply-connected surfaces via partial welding*, SIAM J. Imaging Sci., 13 (2020), pp. 1049–1083, https://doi.org/10.1137/19M125337X.

[9] G. P.-T. Choi and L. M. Lui, *A linear formulation for disk conformal parameterization of simply-connected open surfaces*, Adv. Comput. Math., 44 (2018), pp. 87–114, https://doi.org/10.1007/s10444-017-9536-x.

[10] P. T. Choi, K. C. Lam, and L. M. Lui, *FLASH: Fast landmark aligned spherical harmonic parameterization for genus-0 closed brain surfaces*, SIAM J. Imaging Sci., 8 (2015), pp. 67–94, https://doi.org/10.1137/130950008.

[11] P. T. Choi and L. M. Lui, *Fast disk conformal parameterization of simply-connected open surfaces*, J. Sci. Comput., 65 (2015), pp. 1065–1090, https://doi.org/10.1007/s10915-015-9998-2.

[12] M. S. Floater, *One-to-one piecewise linear mappings over triangulations*, Math. Comput., 72 (2003), pp. 685–696, http://www.jstor.org/stable/4099926.

[13] M. S. Floater and K. Hormann, *Surface parameterization: a tutorial and survey*, in Advances in Multiresolution for Geometric Modelling, Springer Berlin Heidelberg, 2005, pp. 157–186, https://doi.org/10.1007/3-540-26808-1_9.

[14] D. X. Gu, F. Luo, and S.-T. Yau, *Fundamentals of computational conformal geometry*, Math. Comput. Sci., 4 (2010), pp. 389–429, https://doi.org/10.1007/s11786-011-0065-6.

[15] X. Gu, Y. Wang, T. F. Chan, P. M. Thompson, and S.-T. Yau, *Genus zero surface conformal mapping and its application to brain surface mapping*, IEEE Trans. Med. Imaging, 23 (2004), pp. 949–958, https://doi.org/10.1109/TMI.2004.831226.

[16] X. Gu and S.-T. Yau, *Computing conformal structures of surfaces*, Communications in Information and Systems, 2 (2002), pp. 121–146, https://doi.org/10.4310/CIS.2002.v2.n2.a2.

[17] X. Gu and S.-T. Yau, *Global conformal surface parameterization*, in Eurographics Symposium on Geometry Processing, L. Kobbelt, P. Schroeder, and H. Hoppe, eds., SGP '03, 2003, pp. 127–137, http://dl.acm.org/citation.cfm?id=882370.882388.

[18] X. Gu and S.-T. Yau, *Computational Conformal Geometry*, Higher Education Press, 1 ed., 2008.

[19] X. D. Gu, W. Zeng, F. Luo, and S.-T. Yau, *Numerical computation of surface conformal mappings*, Comput. Methods Funct. Theory, 11 (2011), pp. 747–787, https://doi.org/10.1007/BF03321885.

[20] S. Haker, S. Angenent, A. Tannenbaum, R. Kikinis, G. Sapiro, and M. Halle, *Conformal surface parameterization for texture mapping*, IEEE Trans. Vis. Comput. Graph., (2000), pp. 181–189, https://doi.org/10.1109/2945.856998.

[21] K. Hormann, B. Lévy, and A. Sheffer, *Mesh parameterization: Theory and practice*, in ACM SIGGRAPH Course Notes, 2007, https://doi.org/10.1145/1281500.1281510.

[22] W.-Q. Huang, X. D. Gu, T.-M. Huang, S.-S. Lin, W.-W. Lin, and S.-T. Yau, *High performance computing for spherical conformal and Riemann mappings*, Geom. Imag. Comput., 1 (2014), pp. 223–258, https://doi.org/10.4310/GIC.2014.v1.n2.a2.

[23] W.-Q. Huang, X. D. Gu, W.-W. Lin, and S.-T. Yau, *A novel symmetric skew-Hamiltonian isotropic Lanczos algorithm for spectral conformal parameterizations*, J. Sci. Comput., 61 (2014), pp. 558–583, https://doi.org/10.1007/s10915-014-9840-2.

[24] M. K. Hurdal, P. L. Bowers, K. Stephenson, D. W. L. Sumners, K. Rehm, K. Schaper, and D. A. Rottenberg, *Quasi-conformally flat mapping the human cerebellum*, Med. Image Comput. Comput. Assist. Interv., (1999), pp. 279–286, https://doi.org/10.1007/10704282_31.

[25] M. Jin, J. Kim, F. Luo, and X. Gu, *Discrete surface ricci flow*, IEEE Trans. Vis. Comput. Graphics, 14 (2008), pp. 1030–1043, https://doi.org/10.1109/TVCG.2008.57.

[26] M. Jin, Y. Wang, S.-T. Yau, and X. Gu, *Optimal global conformal surface parameterization*, in IEEE Visualization 2004, Oct. 2004, pp. 267–274, https://doi.org/10.1109/VISUAL.2004.75.

[27] B. Lévy, S. Petitjean, N. Ray, and J. Maillot, *Least squares conformal maps for automatic texture atlas generation*, ACM Trans. Graph., 21 (2002), pp. 362–371, https://doi.org/10.1145/566654.566590.

[28] L. M. Lui, K. C. Lam, S.-T. Yau, and X. Gu, *Teichmuller mapping (t-map) and its applications to landmark matching registration*, SIAM J. Imaging Sci., 7 (2014), pp. 391–426, https://doi.org/10.1137/120900186.

[29] P. Mullen, Y. Tong, P. Alliez, and M. Desbrun, *Spectral conformal parameterization*, Comput. Graph. Forum, 27 (2008), pp. 1487–1494.

[30] J. Nocedal and S. J. Wright, *Numerical Optimization*, Springer, New York, NY, 2006.

[31] U. Pinkall and K. Polthier, *Computing discrete minimal surfaces and their conjugates*, Exp. Math., 2 (1993), pp. 15–36.

[32] R. Sawhney and K. Crane, *Boundary first flattening*, ACM Trans. Graph., 37 (2017), pp. 5:1–5:14, https://doi.org/10.1145/3132705.

[33] A. Sheffer and E. de Sturler, *Parameterization of faceted surfaces for meshing using angle-based flattening*, Eng. with Comput., 17 (2001), pp. 326–337.

[34] A. Sheffer, B. Lévy, M. Mogilnitsky, and A. Bogomyakov, *ABF++: Fast and robust angle based flattening*, ACM Trans. Graph., 24 (2005), pp. 311–330.

[35] A. Sheffer, E. Praun, and K. Rose, *Mesh parameterization methods and their applications*, Found. Trends. Comp. Graphics and Vision., 2 (2006), pp. 105–171.

[36] K. Stephenson, *The approximation of conformal structures via circle packing*, in Computational Methods and Function Theory 1997, Proceedings of the Third CMFT conference, World Scientific, 1999, pp. 551–582.

[37] S.-T. Yau and R. Schoen, *Lectures on Differential Geometry*, International Press, 2010.

[38] M.-H. Yueh, W.-W. Lin, C.-T. Wu, and S.-T. Yau, *An efficient energy minimization for conformal parameterizations*, J. Sci. Comput., 73 (2017), pp. 203–227, https://doi.org/10.1007/s10915-017-0414-y.

[39] M. Zhang, R. Guo, W. Zeng, F. Luo, S.-T. Yau, and X. Gu, *The unified discrete surface ricci flow*, Graphical Models, 76 (2014), pp. 321–339, https://doi.org/10.1016/j.gmod.2014.04.008. Geometric Modeling and Processing 2014.